

Heart of Darkness: The Significance of the Zeptobarn Scale for Neutralino Direct Detection

Jonathan L. Feng and David Sanford

*Department of Physics and Astronomy,
University of California, Irvine, California 92697, USA*

(Dated: September 2010)

Abstract

The direct detection of dark matter through its elastic scattering off nucleons is among the most promising methods for establishing the particle identity of dark matter. The current bound on the spin-independent scattering cross section is $\sigma^{\text{SI}} < 10$ zb for dark matter masses $m_\chi \sim 100$ GeV, with improved sensitivities expected soon. We examine the implications of this progress for neutralino dark matter. We work in a supersymmetric framework well-suited to dark matter studies that is simple and transparent, with models defined in terms of four weak-scale parameters. We first show that robust constraints on electric dipole moments motivate large sfermion masses $\tilde{m} \gtrsim 1$ TeV, effectively decoupling squarks and sleptons from neutralino dark matter phenomenology. In this case, we find characteristic cross sections in the narrow range $1 \text{ zb} \lesssim \sigma^{\text{SI}} \lesssim 40 \text{ zb}$ for $m_\chi \gtrsim 70$ GeV. As sfermion masses are lowered to near their experimental limit $\tilde{m} \sim 400$ GeV, the upper and lower limits of this range are extended, but only by factors of around two, and the lower limit is not significantly altered by relaxing many particle physics assumptions, varying the strange quark content of the nucleon, including the effects of galactic small-scale structure, or assuming other components of dark matter. Experiments are therefore rapidly entering the heart of dark matter-favored supersymmetry parameter space. If no signal is seen, supersymmetric models must contain some level of fine-tuning, and we identify and analyze several possibilities. Barring large cancellations, however, in a large and generic class of models, if thermal relic neutralinos are a significant component of dark matter, experiments will discover them as they probe down to the zeptobarn scale.

PACS numbers: 95.35.+d, 12.60.Jv, 14.80.Nb

I. INTRODUCTION

Now is an exciting time for the study of non-baryonic cold dark matter (DM). The existence of DM offers a consistent explanation for a wide variety of astrophysical observations on disparate length scales. At the same time, there are many viable dark matter candidates, motivating a diverse and active research program searching for the direct detection of dark matter scattering off nuclei, the indirect detection of dark matter annihilation or decay products, dark matter production at colliders, and the effects of dark matter particle properties on structure formation and other astrophysical phenomena [1–3].

In this work, we focus on direct detection. We will discuss and present results for both spin-independent and spin-dependent scattering, but will focus particularly on probes of the spin-independent dark matter-nucleon scattering cross section σ^{SI} . Although no definitive signal of dark matter has been established so far, recent results from the DAMA [4], XENON10 [5], CDMS-II [6], CoGeNT [7], and XENON100 [8–10] experiments have sparked great interest. Moreover, significant progress for spin-independent cross sections is expected from several sources, including XENON100 [11], CRESST [12], LUX [13], XMASS [14], mini-CLEAN/DEAP [15], WArP [16], and superCDMS [17]. Current limits are so stringent that there is no agreed upon unit convention for expressing them. We advocate the use of zeptobarns ($1 \text{ zb} = 10^{-9} \text{ pb} = 10^{-45} \text{ cm}^2$), which is more compact and no less transparent than the alternatives. The current limit is $\sigma^{\text{SI}} < 10 \text{ zb}$ for 100 GeV dark matter [6, 8, 10]. In the near future, results from 100 kg-scale detectors may improve this sensitivity by an order of magnitude to the zeptobarn scale. Future ton-scale detectors are being planned to extend sensitivities even beyond that, with the ultimate goal of probing yoctobarn cross sections, where experiments will reach the background-free limit for non-directional detectors imposed by irreducible neutrino backgrounds [18, 19] (and also the outer limits of the metric prefix system).

The single most studied dark matter candidate is the lightest neutralino χ predicted by supersymmetry (SUSY) [20–24]. SUSY provides a solution to the gauge hierarchy problem and gauge coupling unification, and with R -parity conservation, the lightest supersymmetric particle (LSP) is stable. The LSP in SUSY theories is often the lightest neutralino, a mixture of the superpartners of the neutral electroweak gauge and Higgs bosons. It is an excellent DM candidate, not only because SUSY is a well-motivated possibility for new physics, but also because the lightest neutralino is a weakly-interacting massive particle (WIMP), and so naturally has the appropriate thermal relic density.

What are the possible values of σ^{SI} for neutralino dark matter? In full generality, the allowed range varies from very large values that are far above current experimental bounds [25–27] to very small values that are far below the sensitivity of foreseeable experiments [28]. At the same time, there is some sense in which the extreme values occur only in special regions of SUSY parameter space. In this study, we aim to answer a more subtle (and less well-defined) question: what are the *characteristic* values of σ^{SI} for neutralinos? As experiments improve, is every factor-of-ten improvement in σ^{SI} equally important, or are there certain thresholds that should be considered particularly significant? In other words, what is σ^{SI} in the heart of SUSY parameter space?

To answer these questions, one must define preferred models, reducing the general parameter space to some subspace by appealing to some organizational principle. One approach is to work with a low-energy effective theory that includes the dark matter particle but not other supersymmetric degrees of freedom. Dark matter-quark couplings are included with,

for example, four-fermion interactions $\bar{\chi}\chi\bar{q}q$, suppressed by some large mass scale. This approach has the advantage of being model-independent, with results applicable to theories beyond SUSY, and has been adopted in a number of recent studies motivated by the possibility of light (GeV-scale) WIMPs [29–32]. The effective theory approach is, however, inapplicable to the generic SUSY theories of interest to us, in which the dark matter mass is not hierarchically smaller than those of the other superparticles. Also, effective theory studies typically assume that the same operators govern both annihilation and scattering, and so neglect the annihilation to leptons and gauge bosons that may be important in SUSY theories.

Another approach has been to focus on a particular high-energy framework, incorporating constraints from a battery of known observables, and scanning over the reduced, but still high dimensional, parameter space. The most popular framework for these analyses is minimal supergravity (mSUGRA) [33–37], with its cosmologically-preferred regions, including the co-annihilation region at low universal scalar mass m_0 [38, 39], the focus point region at high m_0 [40–42], and the A -funnel region at high $\tan\beta$ [39, 43]. Much work has been devoted to this framework; for recent analyses, see, *e.g.*, Refs. [44–47]. This approach has the advantage that there is a manifestly consistent high-energy formulation throughout parameter space, but there are also drawbacks. The relation of the fundamental high-energy parameters to physical observables, such as superpartner masses, is typically opaque, at least to non-experts. In addition, the framework allows one to relate dark matter properties to $b \rightarrow s\gamma$, the anomalous magnetic moment of the muon, and other *a priori* unrelated observables, and it is not clear how robust these connections should be. Finally, not all of the assumptions of mSUGRA are well-motivated, and it is not always easy to determine how dark matter results would change if some of the assumptions were relaxed or another framework adopted. For example, are the promising predictions for σ^{SI} in focus point supersymmetry necessarily tied to large scalar masses, with their negative implications for colliders? Are there consequences of the connection between sfermion and Higgs masses in mSUGRA that fail to translate to more general theories?

In this work we take a complementary approach. Although we will apply some constraints and characteristics from high-energy motivations, we work in a manifestly low-energy framework, with models defined by a few weak-scale SUSY parameters that are easily related to physical observables, typically the physical masses of certain superpartners. The model framework is particularly well-suited to dark matter studies for the reasons given below, and although specific to SUSY, our results will apply to a broad class of SUSY models. In addition, it will allow us to explore the entire parameter space and understand the physics behind the results in a detailed and relatively transparent way. This in some ways resembles the approach taken in the so-called phenomenological MSSM (pMSSM) [48–51], though our exclusive interest in neutralino dark matter allows for a more directed study of a smaller parameter space. We will find that many correlations found in mSUGRA analyses are broken in these more phenomenological models. In particular, the large signals for direct detection found in focus point supersymmetry are generic and not necessarily tied to large scalar masses, with highly favorable implications for the immediate future of neutralino direct detection.

This paper is organized as follows. In Sec. II, we define our model framework and discuss its input parameters and assumptions. We also discuss the most relevant constraints, notably those from bounds on the electric dipole moments (EDMs) of the electron and neutron. In Sec. III we analyze the dependence of the thermal relic density on the model parameters,

and in Sec. IV we briefly review the form of σ^{SI} and explain its expected behavior in our model framework. In Sec. V we present our main results for the characteristic values of σ^{SI} , the possibility of fine-tuned cancellations, and the implications for dark matter discovery. In Sec. VI we explore the effects of relaxing various particle physics, nuclear physics, and astrophysical assumptions, and we discuss the prospects for spin-dependent scattering in Sec. VII. We summarize our conclusions in Sec. VIII.

II. MODEL FRAMEWORK

A. Input Parameters and Assumptions

We consider SUSY models with minimal field content that are specified by five parameters defined at the weak scale ~ 1 TeV:

$$\tilde{m}, M_1, \mu, m_A, \tan \beta . \quad (1)$$

In order, these are the unified sfermion soft SUSY-breaking mass, the Bino mass, the Higgsino mass, the pseudoscalar Higgs boson mass, and the ratio of Higgs boson expectation values.

The rest of the model is specified by the following three assumptions:

1. Gaugino mass unification. We assume that the gaugino masses are unified at the grand unified theory (GUT) scale, implying the weak-scale gaugino mass relation

$$M_1 : M_2 : M_3 \simeq 1 : 2 : 6 . \quad (2)$$

2. No left-right mixing. We assume there is no significant left-right sfermion mixing, which fixes the “ A -term” tri-linear scalar couplings. For example, the top squark mass matrix simplifies as follows:

$$\begin{pmatrix} m_{\tilde{Q}}^2 + m_t^2 & m_t (A_t - \mu \cot \beta) \\ m_t (A_t - \mu \cot \beta) & m_{\tilde{u}}^2 + m_t^2 \end{pmatrix} \rightarrow \begin{pmatrix} \tilde{m}^2 + m_t^2 & 0 \\ 0 & \tilde{m}^2 + m_t^2 \end{pmatrix} . \quad (3)$$

3. Correct electroweak symmetry breaking. This fixes the soft Higgs scalar mass parameters $m_{H_{u,d}}^2$ and m_{12}^2 through the (tree-level) conditions

$$\mu^2 = \frac{m_{H_d}^2 - m_{H_u}^2 \tan^2 \beta + \frac{1}{2} m_Z^2 (1 - \tan^2 \beta)}{\tan^2 \beta - 1} \quad (4)$$

$$m_A^2 = m_{H_d}^2 + m_{H_u}^2 + 2\mu^2 \quad (5)$$

$$m_{12}^2 = m_A^2 \sin \beta \cos \beta . \quad (6)$$

The model framework defined above is simple, but well-suited to studies of neutralino dark matter. With the assumption of gaugino mass unification, the parameters M_1 , μ , and $\tan \beta$ completely determine the neutralino mass matrix, and so are natural input parameters for this study. These also fix the chargino mass matrix and the gluino mass. The remaining input parameters \tilde{m} and m_A determine the masses of all the remaining particles. In our numerical work, we use SOFTSUSY 3.1.2 [52] to generate the superpartner spectrum and micrOMEGAS 2.2 [53, 54] for relic density and direct detection calculations.

We conclude this subsection with a few further comments about the model parameter space and assumptions. Throughout this analysis, we will assume that the neutralino freezes out with the correct thermal relic density $\Omega_\chi = \Omega_{\text{DM}} \simeq 0.23$. Our results will be remarkably insensitive to this assumption, as discussed in Sec. VIF, but this constraint further simplifies the parameter space. As discussed in Sec. III, for a fixed m_χ , the relic density determines μ up to a discrete choice, which may be taken to be the sign of μ . The input parameters then become

$$\tilde{m}, M_1, \mu, m_A, \tan \beta \xrightarrow{\Omega_\chi=0.23} m_\chi; \tilde{m}, \text{sign}(\mu), m_A, \tan \beta . \quad (7)$$

We will typically plot quantities as functions of m_χ for the two choices of $\text{sign}(\mu)$ and fixed \tilde{m} , m_A , and $\tan \beta$.

The assumption of gaugino mass unification is motivated by the unification of gauge couplings and forces, a key virtue of supersymmetry. It implies that the LSP does not have a large Wino component, which restricts the generality of this analysis. On the other hand, a neutralino with a significant Wino component typically annihilates too efficiently to have the correct thermal relic density, and so our assumption that the neutralino is a thermal relic already disfavors this possibility [55]. Moreover, while neutralino dark matter with non-unified gaugino masses has been discussed [56, 57], and more complicated GUT-breaking schemes are possible [58, 59], the gaugino mass unification scenario used here remains a standard assumption for many high-scale models. However, it is worth noting that our results do not require strict gaugino mass unification, but only that M_2 and M_3 are at least somewhat larger than M_1 .

The assumptions of a unified weak-scale sfermion mass \tilde{m} and negligible left-right mixing are not motivated by high-energy theories of SUSY-breaking; instead, they are motivated by the relative insensitivity of dark matter phenomenology to these assumptions. We will explore the implications of deviations from the above assumptions in Secs. VIB and VIC, respectively. We note here, however, that the dependence on left-right mixing is small, and the neutralino interactions of greatest interest here depend primarily on the squarks in most regions of parameter space¹. In many theories the assumption of a unified squark mass is reasonably accurate, and so this parametrization characterizes these models well, with \tilde{m} playing the role of the characteristic squark mass. Throughout this study, we neglect sfermion flavor mixing and one-loop corrections to sfermion masses, as these are sub-dominant effects in neutralino interactions.

Finally, in our model framework, correct electroweak symmetry breaking is achieved at the expense of unifying the soft Higgs scalar masses with those of the squarks and sleptons. The unification of the Higgs scalar masses with the soft squark and slepton masses is assumed in mSUGRA, but it is one of the least motivated aspects of that framework. Flavor constraints motivate flavor-independent squark and slepton masses, but do not constrain the Higgs scalar masses. Even in GUTs, the Higgs scalars and sfermions are typically in different multiplets. Our assumption regarding the Higgs mass parameters follows other analyses of non-unified Higgs models (NUHM) [60–63].

¹ The relic density only depends strongly on slepton masses in the presence of slepton co-annihilation or very light slepton masses.

B. Constraints

1. Flavor and CP Violation

Theories that introduce new particles at the weak scale run the risk of violating stringent bounds on low-energy flavor- and CP-violating observables. For SUSY, there are mediation mechanisms that lead to generation-independent slepton and squark masses, which allow these theories to satisfy constraints on flavor violation. These will also be satisfied in our models, given the assumption of a unified weak-scale sfermion mass \tilde{m} .

Even in these cases, however, constraints from EDMs, which conserve flavor but violate CP, are not necessarily satisfied. In a general SUSY model, the EDMs of the electron and neutron receive contributions from several sources. Left-right sfermion mixing can lead to CP violation, but this is absent in our model framework. However, there are also contributions from penguin diagrams with gauginos, Higgsinos, and a sfermion of fixed chirality in the loop, which are proportional to $\sin \phi_{\text{CP}}$, where ϕ_{CP} is the mismatch in phases of the gaugino masses and μ parameter. In the gauge eigenstate basis, the dominant diagrams are those with neutral Winos, neutral Higgsinos, and left-handed sfermions in the loop, and a similar one with charged Winos, charged Higgsinos, and sneutrinos in the loop. The first diagram leads to the EDM contribution [64]

$$d_f = \frac{1}{4} e m_f g_2^2 |M_2 \mu| \tan \beta \sin \phi_{\text{CP}} K_N(m_{\tilde{f}_L}^2, |\mu|^2, |M_2|^2), \quad (8)$$

where K_N is a kinematic function that may be approximated as $K_N \sim 1/(16\pi^2 m_{\tilde{f}_L}^4)$ [65].

The current bounds on the electron and neutron EDMs are $d_e < 1.6 \times 10^{-27} e \text{ cm}$ [66] and $d_n < 2.9 \times 10^{-26} e \text{ cm}$ [67]. Assuming $m_u = 3 \text{ MeV}$, $m_d = 5 \text{ MeV}$, the naive quark model relation $d_n = (4d_d - d_u)/3$, and neglecting cancellations between different diagrams, we find

$$\frac{|M_2 \mu|}{m_{\tilde{e}_L}^2} \left[\frac{6.5 \text{ TeV}}{m_{\tilde{e}_L}} \right]^2 \frac{\tan \beta}{10} \sin \phi_{\text{CP}} \lesssim 1 \quad (9)$$

$$\frac{|M_2 \mu|}{m_{\tilde{u}_L}^2} \left[\frac{2.1 \text{ TeV}}{m_{\tilde{u}_L}} \right]^2 \frac{\tan \beta}{10} \sin \phi_{\text{CP}} \lesssim 1 \quad (10)$$

$$\frac{|M_2 \mu|}{m_{\tilde{d}_L}^2} \left[\frac{5.5 \text{ TeV}}{m_{\tilde{d}_L}} \right]^2 \frac{\tan \beta}{10} \sin \phi_{\text{CP}} \lesssim 1. \quad (11)$$

In our model context, with unified scalar masses and $M_2 \simeq 2M_1$, these imply

$$\frac{|M_1 \mu|}{\tilde{m}^2} \left[\frac{9.2 \text{ TeV}}{\tilde{m}} \right]^2 \frac{\tan \beta}{10} \sin \phi_{\text{CP}} \lesssim 1. \quad (12)$$

Note, however, that even without assuming unified slepton and squark masses, the constraints on $m_{\tilde{e}_L}$ and $m_{\tilde{d}_L}$ are similar, and the constraint on $m_{\tilde{u}_L}$ is only somewhat less restrictive.

This is a robust and numerically stringent constraint. Even for the low values $|M_1|, |\mu| \sim 100 \text{ GeV}$ and moderate $\tan \beta \sim 10$, this implies $[1 \text{ TeV}/\tilde{m}]^4 \sin \phi_{\text{CP}} \lesssim 1$. Without a mechanism for aligning the CP-violating phases of different SUSY parameters, we naturally expect $\sin \phi_{\text{CP}} \sim 1$, implying $\tilde{m} \gtrsim 1 \text{ TeV}$. Lower values of \tilde{m} are possible, of course, but require

small values of ϕ_{CP} . As we will see, for $\tilde{m} \gtrsim 1$ TeV, the sfermions are largely decoupled from neutralino interactions, leading to many simplifications in the analysis of neutralino annihilation and scattering. We will present results for a variety of \tilde{m} up to 2 TeV. For this largest value, arbitrary CP-violating phases are allowed for $|M_1|, |\mu| \sim 400$ GeV, and only moderate suppression from $\sin \phi_{\text{CP}} \lesssim 0.2$ is necessary for $|M_1|, |\mu| \lesssim 1$ TeV.

There are several other constraints on flavor and CP violation that are often used to evaluate the viability of SUSY theories. The most notable are the constraints on the anomalous magnetic moment of the muon $a_\mu = (g_\mu - 2)/2$ [68] and the rare decays $b \rightarrow s\gamma$ [69] and $b \rightarrow s\mu^+\mu^-$ [70]. We will neglect these constraints in our analysis, as large sfermion masses motivated by EDMs largely avoid these constraints. The experimental value for $B(b \rightarrow s\gamma)$ is consistent with the SM prediction [71, 72], and $B(b \rightarrow s\mu^+\mu^-)$ has only an upper limit. In both cases, large sfermion masses suppress the SUSY contributions to these observables sufficiently to avoid the constraints. The contribution to a_μ is also suppressed for large sfermion masses, implying that models in our framework do not alleviate the a_μ discrepancy [73], but do not exacerbate it either.

2. Higgs Boson Mass

Since our models are defined in terms of weak-scale parameters, their implications for physical masses are typically clear, and we simply avoid regions of parameter space that are excluded by direct searches for new particles.

The one exception to this rule is the lighter CP-even Higgs boson h . At tree level, $m_h \approx m_Z$ for $\tan \beta \gtrsim 10$ and $m_A \gg m_Z$, and raising it above the LEP bound of 114.4 GeV requires significant one-loop corrections involving top squarks. In the minimal supersymmetric standard model (MSSM), for $m_{\tilde{t}} \lesssim 1$ TeV, significant left-right top squark mixing is required to boost m_h to acceptable levels. In non-minimal models, however, it is possible to increase the lightest Higgs mass in other ways. For example, in the next-to-minimal supersymmetric standard model with a singlet scalar mass of $M_S \sim 5\mu$, the Higgs boson mass may be as large as $m_h \approx 125$ GeV [74], even in cases where the MSSM contribution leaves $m_h \sim m_Z$. Although this introduces a new complex scalar and a neutralino that in general mixes with the rest of the neutralinos, the mass is sufficiently high that it effectively decouples.

For these reasons, we set $m_h = 114.4$ GeV whenever the explicit one-loop corrections of our model are insufficient to drive it above that bound. Note that this redefinition is primarily important for sfermion masses disfavored by the EDM constraints discussed above. In addition, raising the Higgs boson mass generally decreases σ^{SI} , so simply removing models with too-low m_h would, if anything, raise the lower limit of our characteristic range of σ^{SI} .

3. Extrapolation to High Scales

Because these models are specified by weak-scale input parameters, there may be tensions associated with extrapolating them to high energies through renormalization group evolution. Studies of non-unified Higgs models [60, 63] have found that particular choices of μ and m_A produce an unstable Higgs potential at the high scale due to renormalization effects. This problem is generally avoided for $\mu \lesssim 1$ TeV and large m_A . The exact requirement for m_A depends on other model parameters, but $m_A \gtrsim 1$ TeV is generally large enough to avoid

this difficulty. A moderately large value of $m_A \gtrsim 300 - 500$ GeV is also motivated by the desire for a sufficiently large relic density, with low values generically producing overly-efficient annihilation even without resonance effects.

Large gluino masses, with $M_3 \gg m_{\tilde{q}}$, may also imply tachyonic squarks at the high scale. This is not necessarily a problem, as the low-energy theory could be located in a false vacuum that is stable on cosmological time scales, a possibility that has been considered in several studies [75–80]. Of course, all of these potential tensions assume a desert above the TeV scale and may be avoided by the introduction of new heavy fields without altering the phenomenological analysis presented here.

III. RELIC DENSITY

In this study, we require that the neutralino be a thermal relic, with $\Omega_\chi = 0.23$. In this section, we analyze what this constraint implies for the gaugino and Higgsino content of the neutralino LSP, which will help us understand the results for neutralino scattering cross sections.

The mass eigenstate χ is a mixture of gaugino and Higgsino eigenstates given by

$$\chi = a_{\tilde{B}}\tilde{B} + a_{\tilde{W}}\tilde{W} + a_{\tilde{H}_u}\tilde{H}_u + a_{\tilde{H}_d}\tilde{H}_d . \quad (13)$$

With the assumption of gaugino mass unification, $a_{\tilde{W}} \ll 1$, since $M_2 \simeq 2M_1$, and so χ is primarily a Bino-Higgsino mixture. The exact forms for $a_{\tilde{H}_{u,d}}$ are [81]

$$\frac{a_{\tilde{H}_d}}{a_{\tilde{B}}} = \frac{\mu (M_2 - m_\chi) (M_1 - m_\chi) - \frac{1}{2}m_Z^2 \sin 2\beta [(M_1 - M_2) \cos^2 \theta_W + M_2 - m_\chi]}{m_Z (M_2 - m_\chi) \sin \theta_W (\mu \cos \beta + m_\chi \sin \beta)} \quad (14)$$

$$\frac{a_{\tilde{H}_u}}{a_{\tilde{B}}} = \frac{-m_\chi (M_2 - m_\chi) (M_1 - m_\chi) - m_Z^2 \cos^2 \beta [(M_1 - M_2) \cos^2 \theta_W + M_2 - m_\chi]}{m_Z (M_2 - m_\chi) \sin \theta_W (\mu \cos \beta + m_\chi \sin \beta)} . \quad (15)$$

For moderate to large $\tan \beta$, both $\sin 2\beta$ and $\cos^2 \beta$ are small, and the first terms in both numerators are the dominant contributions. This conclusion may be evaded only if $\mu \ll m_Z$, which predicts a light Higgsino and is excluded by LEP bounds, or if M_1 and m_χ are almost exactly degenerate, in which case $\chi \approx \tilde{B}$ and $|a_{\tilde{H}_{u,d}}| \ll 1$. Thus, either $\chi \approx \tilde{B}$ and $|a_{\tilde{H}_{u,d}}| \ll 1$, or χ is a significant mixture of gaugino and Higgsino, and

$$\frac{a_{\tilde{H}_d}}{a_{\tilde{H}_u}} \approx -\frac{\mu}{m_\chi} \sim \mathcal{O}(1) . \quad (16)$$

Given this fact, it is useful to define a single parameter, the ‘‘Higgsino-ness’’

$$a_{\tilde{H}} \equiv \sqrt{a_{\tilde{H}_u}^2 + a_{\tilde{H}_d}^2} , \quad (17)$$

which characterizes the size of both $a_{\tilde{H}_u}$ and $a_{\tilde{H}_d}$ when they are significant. Note that there is also an important dependence on the sign of μ , which determines the relative signs of $a_{\tilde{B}}$ and $a_{\tilde{H}_{u,d}}$. We will generally find solutions to $\Omega_\chi = 0.23$ for both $\mu > 0$ and $\mu < 0$, and so we will present results for both sign choices.

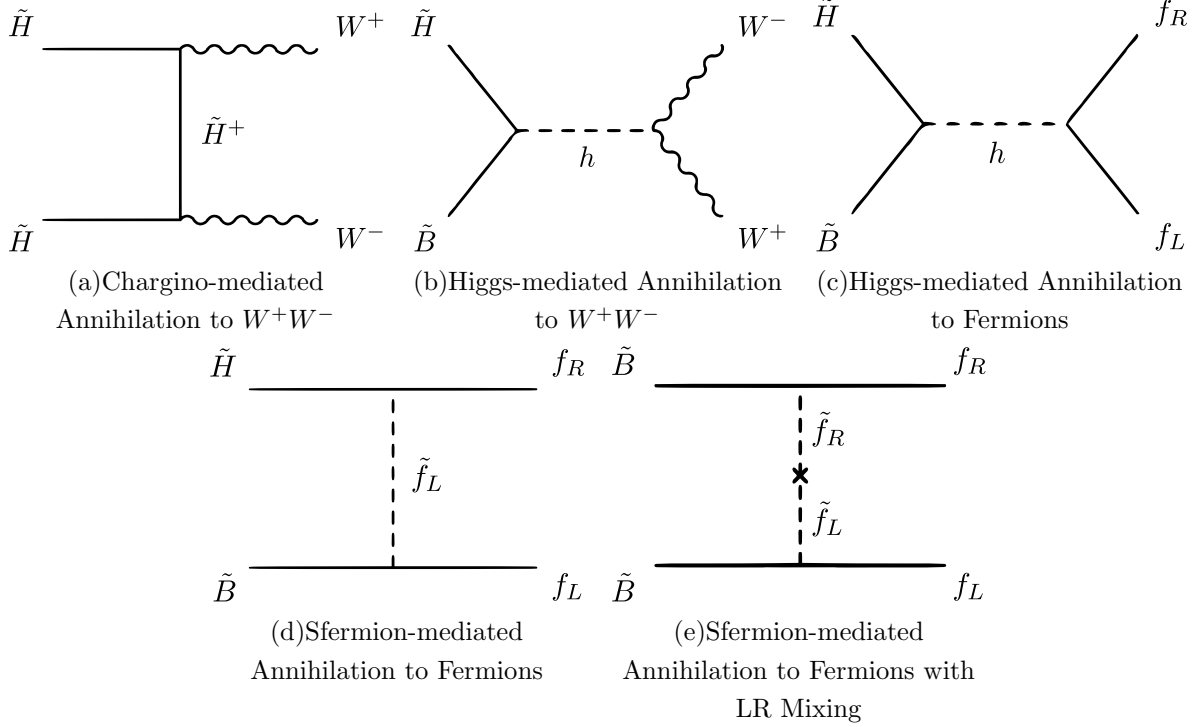


FIG. 1. *Major processes contributing to S-wave $\chi\chi$ annihilation.* The diagrams are labeled with the appropriate gauge eigenstates of the neutralino to highlight the required \tilde{B} and \tilde{H} contributions. In (d) and (e), additional diagrams exist with the exchange $\tilde{B} \leftrightarrow \tilde{H}$ and either $f_L \leftrightarrow f_R$ or $\tilde{f}_L \leftrightarrow \tilde{f}_R$.

Discussion of \tilde{B} - \tilde{H} mixing is familiar from focus point supersymmetry [40, 42] and well-tempered neutralino scenarios [47, 82]. However, we wish to stress that this mixing can be regarded as the key parameter for all choices of parameters², even in the other typically-defined “bulk”, “co-annihilation”, and “A-funnel” dark matter regions discussed in mSUGRA. Our approach, however, effectively separates this mixing from the correspondence of μ with scalar masses found in mSUGRA³, as well as avoiding other effects of running based on high-scale parameters which obfuscate the electroweak scale mass and mixing parameters.

The dominant processes contributing to $\chi\chi$ annihilation in most regions of parameter space are shown in Fig. 1.⁴ The annihilation processes shown in Fig. 1(a)-Fig. 1(d) require a χ with a \tilde{H} component and thus scale with $a_{\tilde{H}}$. The remaining process of Fig. 1(e) does not require a \tilde{H} component, but it is generally suppressed relative to Fig. 1(d) because it requires left-right sfermion mixing.

In Fig. 2, we show what Higgsino content is required to satisfy $\Omega_\chi = 0.23$ as a function of m_χ for fixed $\text{sign}(\mu)$, m_A , and $\tan\beta$. First consider Fig. 2(a). We see that $|a_{\tilde{H}_u}| \sim |a_{\tilde{H}_d}|$ when they are significant, as discussed above. We also see the general trend that $a_{\tilde{H}}$ increases with increasing m_χ , because larger m_χ suppresses annihilation and thus $a_{\tilde{H}}$ must increase to compensate. This rise is interrupted three times: the dip centered at $m_\chi \sim 55$ GeV is caused

² Even models without a unified gaugino mass, the \tilde{W} component of χ is small so long as M_2 is even moderately larger than M_1 .

³ This is a general feature of NUHM scenarios [60, 63]

⁴ Generally other t -channel processes, such as annihilation to ZZ , are sub-dominant. There are, however, specific regions of parameter space where resonant annihilation dominates for an intermediate particle of mass $m_I \approx 2m_\chi$ or where co-annihilation is a major effect. We include all of these effects in our numerical results.

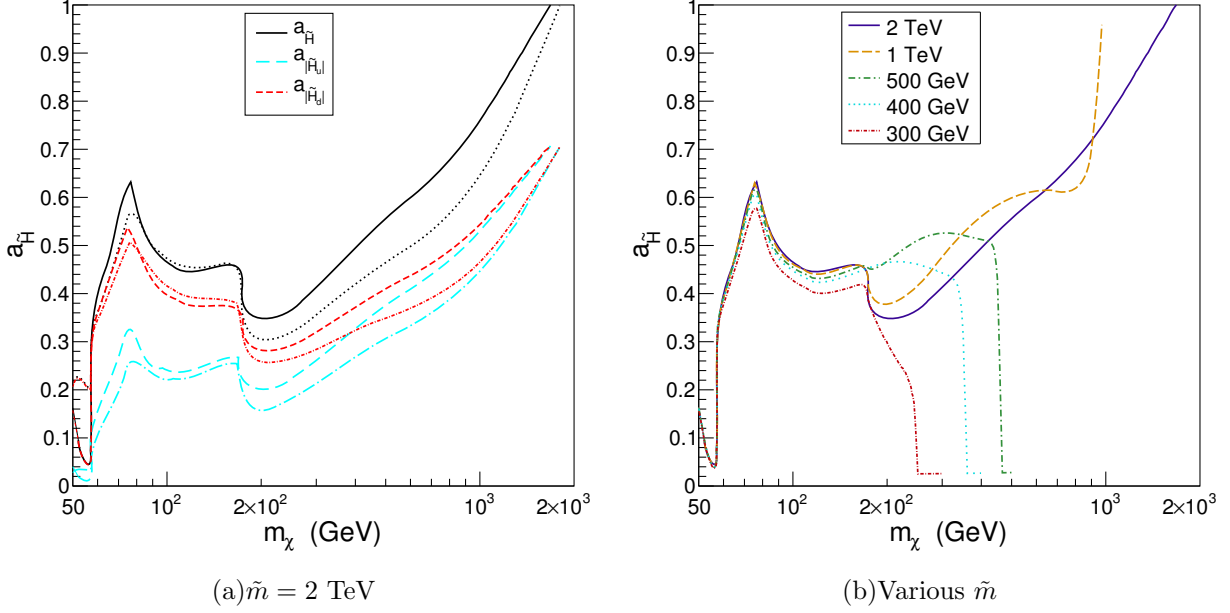


FIG. 2. Higgsino content of the dark matter particle χ as a function of its mass. The Higgsino content is fixed by the requirement $\Omega_\chi = 0.23$. Panel (a) shows $a_{\tilde{H}}$, $|a_{\tilde{H}u}|$, and $|a_{\tilde{H}d}|$ for $\tilde{m} = 2$ TeV and both choices of $\text{sign}(\mu)$. The solid line corresponds to $\mu > 0$ and the dotted line to $\mu < 0$ for $a_{\tilde{H}}$, and the dashed lines correspond to $\mu > 0$ and dot-dashed lines to $\mu < 0$ for $a_{\tilde{H}u,d}$. Panel (b) shows $a_{\tilde{H}}$ for various values of \tilde{m} for $\mu > 0$. For both panels, we fix $m_A = 4$ TeV and $\tan \beta = 10$.

by the h resonance, where the annihilation cross section is enhanced kinematically, and so $a_{\tilde{H}}$ must decrease to compensate dynamically. In addition, there are two notable drops in $a_{\tilde{H}}$ at $m_\chi \approx m_W$ and $m_\chi \approx m_t$, where annihilation is enhanced by the opening of a new annihilation channel. Finally, $a_{\tilde{H}}$ rises to a 1 at $m_\chi \sim 1.7$ TeV. This corresponds to a maximum value of m_χ consistent with the relic density due to decreasing annihilation efficiency as m_χ increases, barring other effects (such as co-annihilation) raising the annihilation rate once more. There is also splitting between the cases of $\mu > 0$ and $\mu < 0$, a result of the aforementioned dependence of $a_{\tilde{H}u,d}$ on the sign of μ and the interplay of these parameters in annihilation.

Figure 2(b) shows the dependence of $a_{\tilde{H}}$ on \tilde{m} . For $m_\chi \leq m_t$ the dependence on \tilde{m} is weak, primarily because the process $\chi\chi \rightarrow W^+W^-$ is independent of \tilde{m} and the sfermion-mediated processes are suppressed relative to this by Yukawa couplings. However, when $\chi\chi \rightarrow t\bar{t}$ is kinematically allowed, the \tilde{t} -mediated process may be similar in magnitude to the Higgs-mediated process. In this case, for $\tilde{m} = 2$ TeV the Higgs-mediated annihilation is significantly larger than the squark contribution and causes a drop in $a_{\tilde{H}}$ across the $t\bar{t}$ threshold; for lighter \tilde{m} the \tilde{t} -mediated contribution cancels the Higgs-mediated contribution to some degree, and thus less of a drop in $a_{\tilde{H}}$ is required. This effect is especially visible in the case of $\tilde{m} = 400$ GeV, where there is very little effect from passing $m_\chi = m_t$ corresponding to nearly exact cancellation between the two processes, and $\tilde{m} = 300$ GeV, where $a_{\tilde{H}}$ again drops significantly because the \tilde{t} -mediated diagram is the dominant contribution. The curves for lower values of \tilde{m} also show the effects of co-annihilation, with the value of $a_{\tilde{H}}$ dropping rapidly to a small value then remaining small up to the kinematic limit.⁵ The actual value

⁵ These effects should also be present for the 1 TeV and 2 TeV curves, but were unreachable due to numerical instabilities in finding a valid window for the relic density at high m_χ .

may vary between zero and a finite but small maximum value based on the value of μ ; we display a value near the maximum to illustrate later effects upon the scattering cross section and to minimize the value of μ in the co-annihilation region at only ~ 2 TeV.

It is instructive to explicitly relate the behavior of $a_{\tilde{H}}$ in Fig. 2 back to the fundamental parameters in the theory. Throughout most of the range of m_χ shown, $0.1 \lesssim a_{\tilde{H}} \lesssim 0.9$, which is associated with the focus point region where $|M_1| \sim |\mu|$ to allow for significant mixing. In particular, for that range of $a_{\tilde{H}}$, $0.67 \lesssim |M_1/\mu| \lesssim 1.05$. The significant drops due to the Higgs resonance and co-annihilation correspond to a nearly pure \tilde{B} LSP with $|M_1| \gg |\mu|$. We have set $m_A = 4$ TeV, so there is no A -funnel region present in Fig. 2, but for a lower value of m_A there would be a small region of significantly suppressed $a_{\tilde{H}}$ at $m_\chi \sim m_A/2$. The presence of an A -funnel effectively obfuscates other interesting features in the behavior of $a_{\tilde{H}}$ and ultimately σ^{SI} , and this is part of our motivation for examining a large base value of m_A throughout. The behavior for lower values of m_A is discussed in Sec. VIA.

IV. SPIN-INDEPENDENT DIRECT DETECTION

A. General Formalism

The relevant interactions for spin-independent scattering are four-fermion neutralino-nucleon effective operators. Following closely the notation of Ref. [54], these are

$$\mathcal{L}^{\text{SI}} = \lambda_N \bar{\psi}_\chi \psi_\chi \bar{\psi}_N \psi_N , \quad (18)$$

where $N = p, n$, and λ_N is determined by the underlying SUSY interactions that produce the operator. For a nucleus with charge Z and A total nucleons, this leads to a total cross section of

$$\sigma^{\text{SI}} = \frac{4\mu_\chi^2}{\pi} [\lambda_p Z + \lambda_n (A - Z)]^2 , \quad (19)$$

where $\mu_\chi = m_\chi M_A / (m_\chi + M_A)$ is the reduced mass of the χ -nucleon system. For neutralinos, typically $\lambda_p \sim \lambda_n$, and the cross-sections add coherently, so the cross section can usually be reduced to

$$\sigma^{\text{SI}} \approx \frac{4\mu_\chi^2}{\pi} \lambda_p^2 A^2 . \quad (20)$$

The dominant diagrams contributing to σ^{SI} for mixed $\tilde{B} - \tilde{H}$ are shown in Fig. 3, all of which have different coupling strengths for different quark flavors. Because of this, the cross-section has a strong dependence on the individual contributions of each quark flavor to the current $\bar{\psi}_q \psi_q$ in the nucleon. This quantity is parameterized as

$$\langle N | m_q \bar{\psi}_q \psi_q | N \rangle = f_q^N M_N , \quad (21)$$

where M_N is the nucleon mass and f_q^N is interpreted as the contribution of the quark q to the nucleon mass.

Using this parameterization, the coupling of the neutralino to the nucleon becomes

$$\frac{\lambda_N}{m_N} = \sum_{q=1}^6 f_q^N \frac{\lambda_q}{m_q} , \quad (22)$$

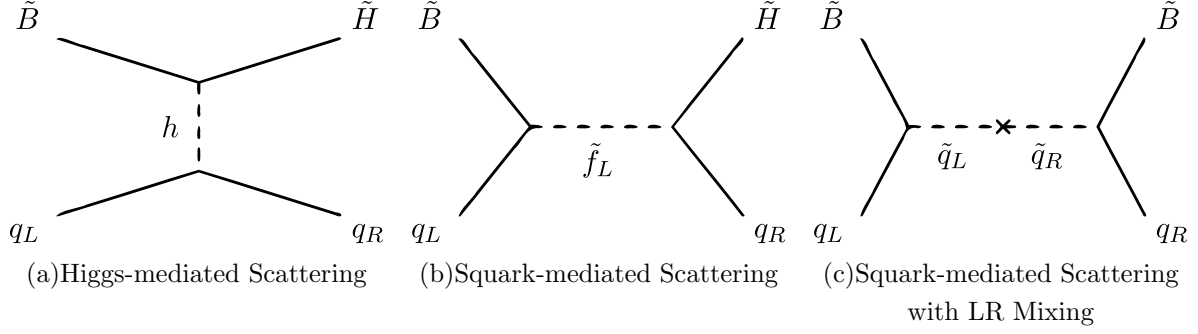


FIG. 3. *Major processes contributing to σ^{SI} .* The diagrams are labeled with the appropriate gauge eigenstates, and additional diagrams exist with the exchange $\tilde{B} \leftrightarrow \tilde{H}$ and either $f_L \leftrightarrow f_R$ or $\tilde{f}_L \leftrightarrow \tilde{f}_R$. This exchange is independent in (a) and correlated in (b) and (c).

where λ_q is the effective coupling of each individual quark to the neutralino through an operator analogous to Eq. (18) above with $N \rightarrow q$. For the light quarks u , d , and s , the values of f_q^N can be taken from meson scattering experiments or lattice results. For the heavy quarks $Q = c, b, t$, the entire contribution derives from loop contributions through gluon exchange, and has the value [83]

$$f_Q^N = \frac{2}{27} \left(1 - \sum_{q=u,d,s} f_q^N \right). \quad (23)$$

The parameters $f_{u,d}^N$ are reasonably well-known and small, but f_s^N has been the subject of debate due to varying experimental and lattice results. In our analysis we take the values of $f_{u,d}^N$ from Ref. [54] and use the lattice result given in Ref. [84] for f_s^N , which gives

$$f_d^p = 0.033, \quad f_u^p = 0.023, \quad f_s^p = 0.05 \quad (24)$$

$$f_d^n = 0.042, \quad f_u^n = 0.018, \quad f_s^n = 0.05. \quad (25)$$

These values imply $f_Q^p = f_Q^n = 0.066$, so the heavy quark contribution is quite important to the overall value of σ^{SI} . We will discuss the impact of variations from these values in Sec. VI E.

B. Neutralino-Quark Couplings

The coefficients for spin-independent scattering of neutralinos off individual quarks, λ_q , have the form [85]

$$\begin{aligned} \lambda_u = & -\frac{g^2}{2(m_{\tilde{u}_i}^2 - m_\chi^2)} \left[\left(\frac{1}{2}a_{\tilde{W}} + \frac{1}{6}\tan\theta_W a_{\tilde{B}} \right) U_{i1}^{(\tilde{u})*} + \frac{m_u a_{\tilde{H}_u}}{2m_W \sin\beta} U_{i2}^{(\tilde{u})*} \right] \\ & \times \left(\frac{m_u a_{\tilde{H}_u}}{2m_W \sin\beta} U_{i1}^{(\tilde{u})} - \frac{2}{3}\tan\theta_W a_{\tilde{B}} U_{i2}^{(\tilde{u})} \right) \\ & - \frac{g^2 m_u}{4m_W \sin\beta} (a_{\tilde{W}} - \tan\theta_W a_{\tilde{B}}) \left[(a_{\tilde{H}_d} \cos\alpha \sin\alpha + a_{\tilde{H}_u} \cos^2\alpha) \frac{1}{m_h^2} \right. \\ & \left. + (-a_{\tilde{H}_d} \cos\alpha \sin\alpha + a_{\tilde{H}_u} \sin^2\alpha) \frac{1}{m_H^2} \right] \end{aligned} \quad (26)$$

$$\begin{aligned} \lambda_d = & -\frac{g^2}{2(m_{\tilde{d}_i}^2 - m_\chi^2)} \left[\left(-\frac{1}{2}a_{\tilde{W}} + \frac{1}{6}\tan\theta_W a_{\tilde{B}} \right) U_{i1}^{(\tilde{d})*} + \frac{m_d a_{\tilde{H}_d}}{2m_W \cos\beta} U_{i2}^{(\tilde{d})*} \right] \\ & \times \left(\frac{m_d a_{\tilde{H}_d}}{2m_W \cos\beta} U_{i1}^{(\tilde{d})} + \frac{1}{3}\tan\theta_W a_{\tilde{B}} U_{i2}^{(\tilde{d})} \right) \\ & + \frac{g^2 m_d}{4m_W \cos\beta} (a_{\tilde{W}} - \tan\theta_W a_{\tilde{B}}) \left[(a_{\tilde{H}_u} \cos\alpha \sin\alpha + a_{\tilde{H}_d} \sin^2\alpha) \frac{1}{m_h^2} \right. \\ & \left. + (-a_{\tilde{H}_u} \cos\alpha \sin\alpha + a_{\tilde{H}_d} \cos^2\alpha) \frac{1}{m_H^2} \right], \end{aligned} \quad (27)$$

where α is the CP-even Higgs mixing angle, $m_{\tilde{q}_i}$ and $U_{ij}^{(\tilde{q})}$ are the squark masses and mixing matrix defined by

$$M_{\tilde{q}}^2 = U^{(\tilde{q})\dagger} \begin{pmatrix} m_{\tilde{q}_1}^2 & 0 \\ 0 & m_{\tilde{q}_2}^2 \end{pmatrix} U^{(\tilde{q})}, \quad (28)$$

and there is an implicit sum over i . The $m_{h,H}$ -dependent terms of Eqs. (26) and (27) arise from the diagram of Fig. 3(a), and the $m_{\tilde{q}}$ -dependent terms are from the diagrams of Fig. 3(b) and Fig. 3(c). The coupling for heavier quarks can be determined by simple mass replacement in the appropriate equation. These couplings can be altered somewhat by the inclusion of an additional CP-violating phase in the Higgs sector [86], but we will not address this contribution in this work.

We have assumed $M_{\tilde{q}}^2 = \tilde{m}^2 \mathbf{1}$, which implies $U^{(\tilde{q})} = \mathbf{1}$. It is instructive to consider the limit $m_H \sim m_A \rightarrow \infty$. In this case, $\alpha \sim \beta - \pi/2 < 0$, and the couplings simplify to

$$\lambda_u = -\frac{g^2 m_u (a_{\tilde{W}} - \tan\theta_W a_{\tilde{B}})}{4m_W \sin\beta} \left[\frac{a_{\tilde{H}_u}}{\tilde{m}^2 - m_\chi^2} + \frac{-a_{\tilde{H}_d} \sin\beta \cos\beta + a_{\tilde{H}_u} \sin^2\beta}{m_h^2} \right] \quad (29)$$

$$\lambda_d = \frac{g^2 m_d (a_{\tilde{W}} - \tan\theta_W a_{\tilde{B}})}{4m_W \cos\beta} \left[\frac{a_{\tilde{H}_d}}{\tilde{m}^2 - m_\chi^2} + \frac{-a_{\tilde{H}_u} \sin\beta \cos\beta + a_{\tilde{H}_d} \cos^2\beta}{m_h^2} \right]. \quad (30)$$

The dependence of λ_q on the Higgsino-ness of the neutralino is manifest, with the coupling vanishing for a pure \tilde{B} or \tilde{H} and the maximum value generically achieved for a well-mixed case. Moreover, it is clear that the squark-mediated diagrams are sub-dominant relative to

the Higgs-mediated diagrams, except when $m_d^2 - m_\chi^2 \sim m_h^2$, in which case their contributions become comparable.

Assuming the Higgs-mediated contributions dominate, there is also clearly a dependence on the relative signs of $a_{\tilde{H}_u}$ and $a_{\tilde{H}_d}$, both in the Higgs-mediated contribution alone and in the relative sign between the contributions. This contribution is either a suppression or enhancement in both types of quarks at once, with a characteristic suppression of the couplings when $a_{\tilde{H}_{u,d}}$ have the same sign relative to the values with opposite signs. Moreover, in the same-sign case there is the possibility of cancellation between the two contributions further reducing σ^{SI} , while for the opposite-sign case there is an enhancement. Equation (16) implies that $a_{\tilde{H}_u}$ and $a_{\tilde{H}_d}$ will have the same sign for $\mu < 0$ and opposite signs for $\mu > 0$. This means there will be a characteristic enhancement in the $\mu > 0$ value of σ^{SI} over the $\mu < 0$ value for a given set of other parameters. This holds true over most of our parameter space. The most significant exception is when the LSP is a nearly pure Bino and Eq. (16) doesn't hold. In this case, $a_{\tilde{H}} \ll 1$, which causes a severe suppression in λ_q and thus in σ^{SI} as well, regardless of the sign of μ .

V. CHARACTERISTIC SPIN-INDEPENDENT CROSS SECTIONS

We are now ready to present our main results for the spin-independent neutralino-nucleon cross sections in our model framework. In Fig. 4, we present the predicted values for σ^{SI} as a function of m_χ for models with the correct thermal relic density $\Omega_\chi = 0.23$. Results are given for various \tilde{m} , both signs of μ , $m_A = 4$ TeV, and $\tan \beta = 10$. The dependence on m_A and $\tan \beta$ is examined in Sec. VI A.

A. Characteristic Features

Figure 4 has a number of striking characteristic features. First, aside from the results for $\tilde{m} = 300$ GeV and $\mu < 0$, which we discuss below, the predicted cross sections σ^{SI} are almost independent of dark matter mass. For $\tilde{m} = 2$ TeV, this may be understood as follows: in this case, sfermions are decoupled, and scattering occurs through the light Higgs boson. These cross sections scale as $\sim a_{\tilde{H}}^2/m_h^4$, but the Higgsino-ness is typically constrained by the thermal relic density to the range $0.3 \lesssim a_{\tilde{H}} \lesssim 0.8$, as shown in Fig. 2, and the Higgs boson mass is constrained to the narrow range $114.4 \text{ GeV} < m_h \lesssim 130 \text{ GeV}$, given the current experimental bound. As a result, for $\tilde{m} = 2$ TeV, $m_A = 4$ TeV and $\tan \beta = 10$, σ^{SI} is in the narrow range $2 \text{ zb} < \sigma^{\text{SI}} < 20 \text{ zb}$ for all $m_\chi \gtrsim 70 \text{ GeV}$.

Perhaps more surprising is that this behavior persists to much lower sfermion masses. As evident in Fig. 4, even for $\tilde{m} = 400$ GeV, the characteristic range of σ^{SI} is extended only to $1 \text{ zb} < \sigma^{\text{SI}} < 40 \text{ zb}$ for $m_\chi \gtrsim 70 \text{ GeV}$. Such low values of \tilde{m} are not far from current bounds on squark masses from direct searches at the Tevatron [87]. In this sense, current bounds from colliders already imply that sfermions are essentially decoupled from neutralino phenomenology, except in fine-tuned cases discussed below, greatly simplifying SUSY parameter space and focusing predictions.

In more detail, we also see that the σ^{SI} curves of Fig. 4 show a generic similarity to the $a_{\tilde{H}}$ curves of Fig. 2 as suggested by the form of the coefficients λ_q . There is a peak and subsequent drop-off in the distribution at $m_\chi \sim m_W$ and again at $m_\chi \sim m_t$ corresponding to the fluctuations in the $a_{\tilde{H}}$, and most of the curves demonstrate some rise after $m_\chi \sim m_t$.

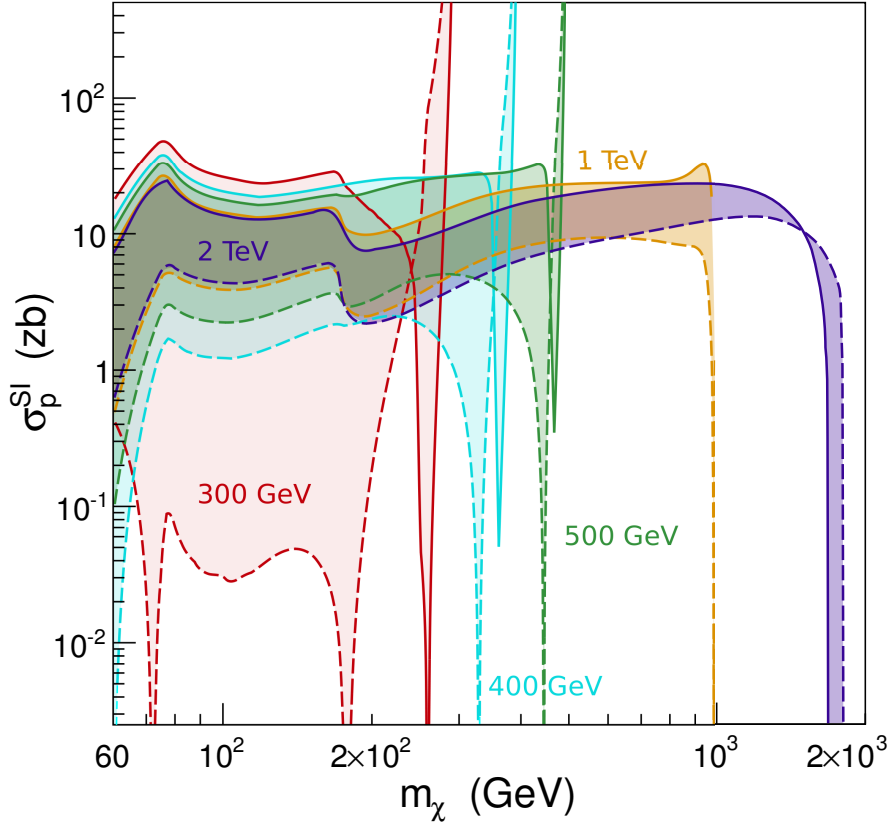


FIG. 4. *Spin-independent neutralino-nucleon cross sections.* The cross sections σ^{SI} for models with thermal relic density $\Omega_\chi = 0.23$ as functions of neutralino mass m_χ for the various sfermion masses indicated, $\mu > 0$ (solid) and $\mu < 0$ (dashed), $m_A = 4$ TeV and $\tan \beta = 10$. The shaded region between the solid and dashed curves are obtained for complex values of μ that interpolate between the two real values (see Sec. VID).

For $\tilde{m} = 2$ TeV, σ^{SI} drops off at $m_\chi \lesssim 1.7$ TeV as the neutralino becomes nearly pure \tilde{H} . This is because, in the absence of left-right mixing, the dominant scattering processes require χ to have both significant \tilde{B} and \tilde{H} components as shown in Fig. 3.

Finally, for the reasons discussed in Sec. IV B, the value of σ^{SI} for $\mu < 0$ is almost always suppressed relative to that for $\mu > 0$, usually by at least a factor of two. This effect is enhanced for lower \tilde{m} . This follows directly from the form of λ_q above, with decreasing scalar masses bringing greater enhancement for $\mu > 0$ and greater suppression for $\mu < 0$. Although this relation is not strictly true, due to the more pronounced dip in $\sigma^{\text{SI}}|_{\mu < 0}$ for larger \tilde{m} at $m_\chi \sim m_t$, the suppression in σ^{SI} for $\tilde{m} = 2$ TeV is relatively minor.

B. Fine-tuned Cancellations

The cross section σ^{SI} may move outside its characteristic range in certain fine-tuned regions. Given our simple, phenomenological model framework, we may identify the fine-tuned possibilities relatively easily.

First, for $50 \text{ GeV} \lesssim m_\chi \lesssim 65 \text{ GeV}$, σ^{SI} may be suppressed by orders of magnitude,

consistent with the suppression of $a_{\tilde{H}}$ shown in Fig. 2. This behavior is visible at the left-hand edge of Fig. 4. For these masses, $m_h \approx 2m_\chi$ to within a few GeV, $\chi\chi$ annihilation is enhanced by the Higgs boson resonance, and so the correct thermal relic density is obtained even for Bino-like neutralinos. In this fine-tuned case, σ^{SI} may be so small that neutralinos will escape all direct detection searches for the foreseeable future. Note, however, that this possibility is disfavored not only by fine-tuning, but will soon be probed by chargino and gluino searches, since these are sensitive to LSP masses around 50 GeV under the assumption of gaugino mass unification.

The regions in Fig. 4 must, of course, be cut off at $m_\chi = \tilde{m}$; for $m_\chi > \tilde{m}$, the neutralino is not the LSP. In fact, the behavior of σ^{SI} changes significantly for values $\sim 20\text{--}50$ GeV below \tilde{m} . The reason for this is that the annihilation is enhanced for $m_\chi \sim \tilde{m}$ by co-annihilation effects, quickly suppressing the relic density once co-annihilation becomes important. Although $a_{\tilde{H}}$ may compensate for this effect, the $a_{\tilde{H}}$ curves in Fig. 2(b) demonstrate rapid change as m_χ approaches the end of the curve, indicating that χ will quickly become a pure \tilde{B} or \tilde{H} to suppress annihilation somewhat before $m_\chi = \tilde{m}$. After this point the correct relic density is unattainable. However, in contrast to typical assumptions regarding co-annihilation, the value of σ^{SI} may actually increase greatly approaching the kinematic limit. This is due to the unified sfermion mass, which results in co-annihilation with squarks as well as sleptons, and thus there is a near-resonance enhancement of σ^{SI} if $a_{\tilde{H}}$ remains small but constant. This effect is largely illustrative, as most realistic scenarios predict slepton masses at least somewhat smaller than squark masses, and the exact values of σ^{SI} are undetermined as the exact value of $a_{\tilde{H}}$ is not set in the co-annihilation region.

For $\tilde{m} = 1$ TeV, 500 GeV, and 400 GeV, there is a small region with a significantly suppressed value of σ^{SI} in the $\mu < 0$ curves for m_χ just below the co-annihilation cutoff. To understand this feature, consider the form of λ_d from Eq. (29). For large $\tan\beta$, $\sin\alpha$ is small and negative, so $\lambda_d = 0$ for

$$m_d^2 - m_\chi^2 \sim -\frac{a_{\tilde{H}_d}}{a_{\tilde{H}_u} \cos\alpha \sin\alpha} m_h^2 \sim \frac{2\mu}{m_\chi \sin 2\alpha} m_h^2 \sim 10m_h^2 \quad (31)$$

for characteristic values of α and μ/m_χ . For even moderately larger values of \tilde{m} , the \tilde{q} -mediated contribution is sub-dominant until m_χ becomes sufficiently large. For $m_\chi^2 \sim m_d^2 - 10m_h^2$, λ_d vanishes at a specific value then flips sign for larger values of m_χ . For $\lambda_u = 0$, the corresponding condition is

$$m_u^2 - m_\chi^2 \sim -\frac{1}{\cos^2\alpha - \frac{\mu}{m_\chi} \cos\alpha \sin\alpha} m_h^2, \quad (32)$$

so λ_u cannot vanish for $m_\chi < \tilde{m}$. The highly suppressed region is the result of cancellation between contributions from up-type and down-type quarks in this region, the result of the squark-mediated contributions to σ^{SI} in Fig. 3 becoming similar in size to the Higgs-mediated contribution for $m_\chi \sim \tilde{m}$.

In fact, this effect explains the suppression of σ^{SI} for $\tilde{m} = 300$ GeV across a large range of m_χ . In this case $\tilde{m}^2 \sim 10m_h^2$ regardless of the value of m_χ , so the Higgs- and squark-mediated contributions are always comparable. This leads to a general suppression in σ^{SI} until $m_\chi \sim \tilde{m}$, where σ^{SI} actually increases to the characteristic value because the squark-mediated contribution dominates.

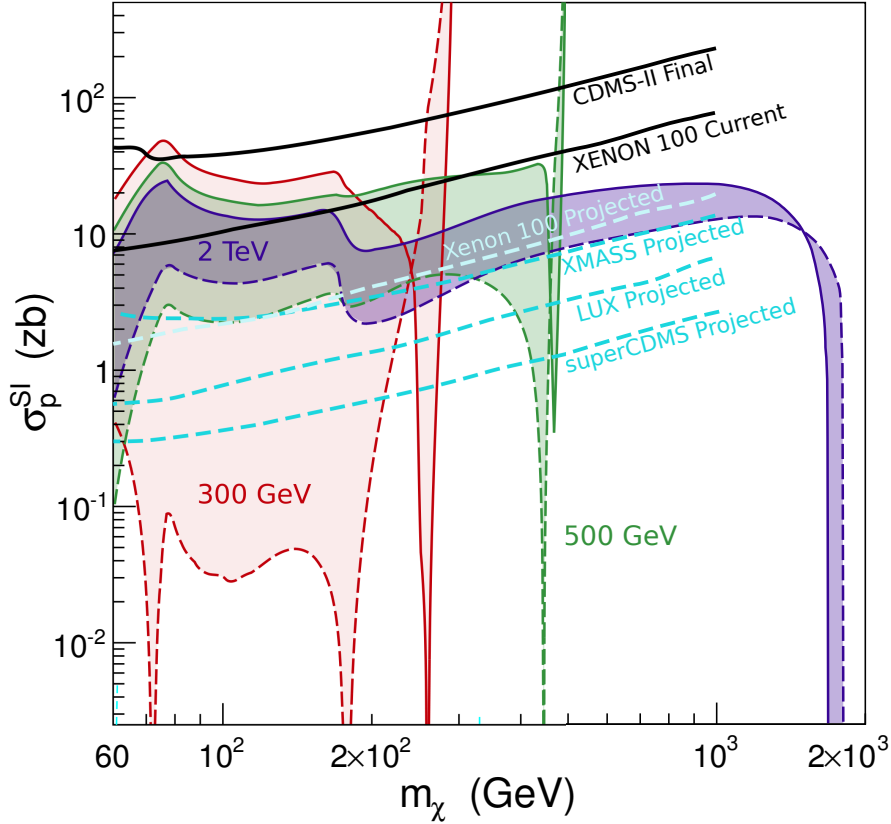


FIG. 5. *Theoretical predictions for σ^{SI} and experimental bounds.* The shaded regions are as in Fig. 4, along with various current and project bounds. The current upper limit from CDMS [6] skirts our projected cross sections, and recent XENON100 [10] results have begun to constrain our characteristic region. Most or all of the characteristic regions will be probed by the projected near future sensitivities of XENON100 [11], XMASS [14], LUX [88, 89], and superCDMS with 100 kg fiducial mass at SNOLAB [17].

C. Prospects for Discovery

The primary implication of Fig. 4 is that simple SUSY models typically predict $1 \text{ zb} \lesssim \sigma^{SI} \lesssim 40 \text{ zb}$. This prediction becomes even more narrow for large sfermion masses, which are required for $\mathcal{O}(1)$ phases to be consistent with the EDM constraints discussed in Sec. II B 1. The reason lies in the decoupling of squark-mediated processes in Fig. 3(b) and Fig. 3(c), leaving only the Higgs mediated process in Fig. 3(a).

Such cross sections are just below current bounds for most masses, and recent XENON100 [10] results have begun probing our characteristic region. These predictions along with current experimental bounds and expected near future sensitivities, are shown in Fig. 5. We see that the expected range is just below current limits, but the characteristic range will be probed by experiments that reach the zeptobarn scale in the near future.

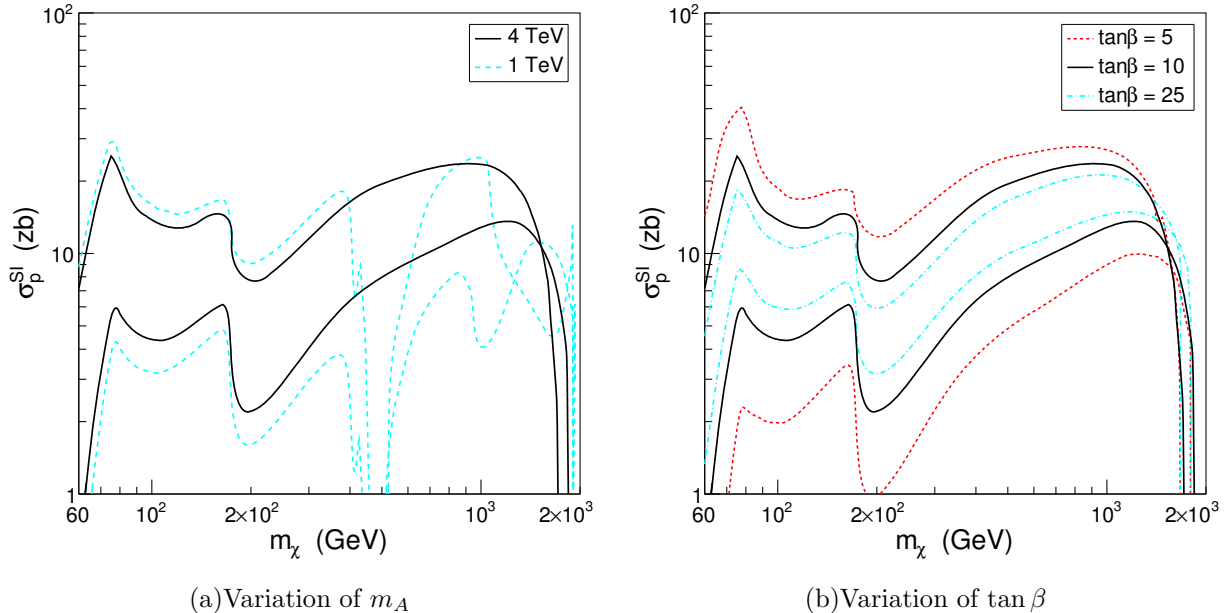


FIG. 6. Dependence of σ^{SI} on Higgs potential parameters. The cross section σ^{SI} is given for various m_A and $\tan\beta = 10$ in (a) and various $\tan\beta$ and $m_A = 4$ TeV in (b). In all cases, $\tilde{m} = 2$ TeV, and the upper contour is for $\mu > 0$ and the lower contour is for $\mu < 0$.

VI. DEPENDENCE ON MODEL PARAMETERS AND ASSUMPTIONS

In this section we examine the effects of relaxing several of our particle physics model assumptions, varying the strange quark content of the nucleon, and modifying astrophysical inputs that enter our analysis.

A. Variations in m_A and $\tan\beta$

As discussed in Sec. II, our Higgs potential is parameterized by μ , m_A , and $\tan\beta$. After imposing the constraint $\Omega_\chi = 0.23$, the magnitude of μ is determined, and we have discussed the dependence of our results on the choice of $\text{sign}(\mu)$. Figure 6 shows the effects of varying the remaining input parameters of the Higgs potential: m_A and $\tan\beta$.

As noted in Sec. II B 3, overly efficient annihilation and stability of the Higgs potential at high scales generally motivate at least partially decoupled values of $m_A \gtrsim 300 - 500$ GeV. Up to this point in our analysis, we have considered the complete decoupling limit with $m_A = 4$ TeV. Here we consider the effects of a lower value of m_A by showing results for $m_A = 1$ TeV in Fig. 6(a). The primary effect is a strong suppression of σ^{SI} for $m_\chi \sim m_A/2$. For such values of m_χ , $\chi\chi$ annihilation is enhanced by the S -wave A resonance. This effect is similar to the light Higgs resonance discussed previously, as it forces χ to be nearly pure \tilde{B} to compensate for the strong annihilation enhancement and thus suppressed σ^{SI} . This behavior is present in the A -funnel region at large $\tan\beta$ in mSUGRA, but we see here that it is generically possible for all values of $\tan\beta$ and the position in parameter space is generically unconnected to the sfermion masses. There is also a slightly less pronounced resonance involving the heavier CP-even Higgs which produces the less distinct second downward

spike for the $\mu < 0$ curve. The value of σ^{SI} drops somewhat for $m_\chi > 1$ TeV due to the availability of heavy Higgs final states in annihilation. The availability of AA final states also increases the maximum value of m_χ by increasing annihilation efficiency. Finally, there is a slight broadening of the values of σ^{SI} due to the increased contribution from scattering through the heavy CP-even Higgs; this effect will become more pronounced for even lower m_A , but the aforementioned lower limit on m_A prevents this effect from causing serious suppression.

For variation in $\tan \beta$, the characteristic range of values for σ^{SI} narrows for larger values of $\tan \beta$. This can be understood as follows: for the neutralino mass matrix, in the limit $\tan \beta \rightarrow \infty$, the sign of μ may be switched by the field redefinition $\tilde{H}_d \rightarrow -\tilde{H}_d$ without affecting other matrix entries. We therefore expect the $\mu > 0$ and $\mu < 0$ predictions to become similar for large $\tan \beta$. Conversely, as shown in Fig. 6(b), the range of σ^{SI} becomes wider for lower values of $\tan \beta$; for $\tan \beta = 5$, roughly the minimum value allowed by null results from Higgs boson searches, the lowest value of σ^{SI} is reduced by a factor ~ 2 from the $\tan \beta = 10$ results.

For very large $\tan \beta$ and low value of m_A , there is a possibility of a general suppression due to cancellation between light and heavy Higgs contributions to σ^{SI} . For $\tan \beta \rightarrow \infty$, $\sin \alpha \rightarrow 0$ and $\cos \alpha \rightarrow 1$. Then, if the squark mediated contributions are neglected, the couplings in Eqs. (26) and (27) become

$$\lambda_u \simeq -\frac{g^2 m_u}{4m_W \sin \beta} (a_{\tilde{W}} - \tan \theta_W a_{\tilde{B}}) \frac{a_{\tilde{H}_u}}{m_h^2} \quad (33)$$

$$\lambda_d \simeq \frac{g^2 m_d}{4m_W \cos \beta} (a_{\tilde{W}} - \tan \theta_W a_{\tilde{B}}) \frac{a_{\tilde{H}_d}}{m_H^2}. \quad (34)$$

Then, under the (very) rough assumption of equal portion of up- and down-type quarks in the nucleon, there is a cancellation between these contributions when $\lambda_u/m_u + \lambda_d/m_d \simeq 0$, which gives

$$\frac{m_H}{m_h} \simeq \sqrt{\frac{a_{\tilde{H}_d}}{a_{\tilde{H}_u}}} \tan \beta \simeq \sqrt{-\frac{\mu}{m_\chi}} \tan \beta \quad (35)$$

This allows for a possible cancellation for $\mu < 0$ with little dependence on m_χ . For $\tan \beta = 10$ the required value is $m_H \simeq m_A \sim 300 - 400$ GeV, which strains the relic density calculation; however, for $\tan \beta = 50$, the cancellation occurs at larger values of $m_A \sim 700 - 800$ GeV. However, even for large $\tan \beta$ significant suppression only occurs at very specific values of m_A , as for lower values of m_A the contribution to scattering from the heavy Higgs dominates the cross section.

B. Un-unified Sfermion Masses

Although convenient for studying the general behavior of σ^{SI} , our assumption of a unified weak-scale sfermion mass is not motivated by a connection to a high-energy theory. Indeed, most high energy theories predict $m_{\tilde{t}} < m_{\tilde{q}}$, either resulting from a unified scalar mass at the GUT scale, as in mSUGRA, or as a remnant of sfermion masses generated by gauge dynamics, as in gauge-mediated supersymmetry breaking models or anomaly-mediated supersymmetry breaking models with a unified scalar mass.

To explore the consequences of lighter sleptons, in Fig. 7(a), we compare our standard scenario with $\tilde{m} = 1$ TeV to a scenario with a unified weak-scale squark mass $m_{\tilde{q}} = 1$ TeV

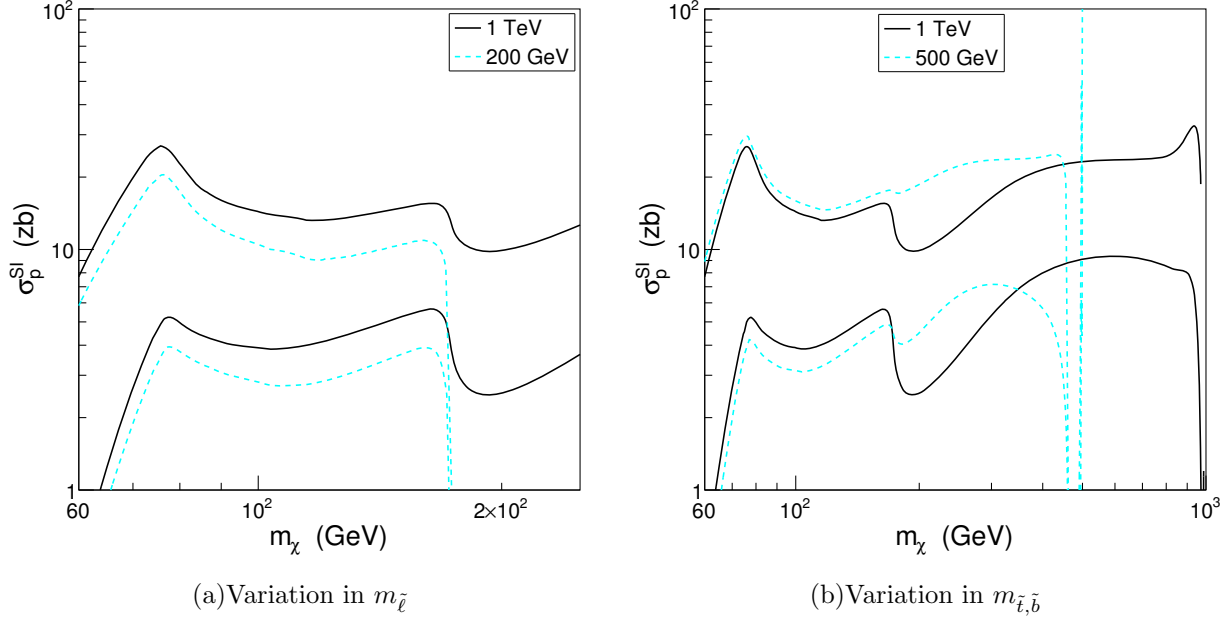


FIG. 7. *Dependence of σ^{SI} on the unified sfermion mass assumption.* Cross sections σ^{SI} are given for $\mu > 0$ (upper) and $\mu < 0$ (lower), $m_A = 4$ TeV, and $\tan \beta = 10$. Sfermions masses that are not specified are set to $\tilde{m} = 1$ TeV.

and a separate unified weak-scale slepton mass $m_{\tilde{\ell}} = 200$ GeV. The lower value for $m_{\tilde{\ell}}$ reduces the value of σ^{SI} across the entire range of masses by $\sim 20 - 30\%$. This is due to the effect of t -channel $\tilde{\ell}$ -mediated diagrams in χ annihilation reducing $a_{\tilde{H}}$ and providing no additional to σ^{SI} . As expected, the spike of high σ^{SI} associated with squark co-annihilation in Fig. 4 figures is absent. While it is possible that even smaller values of $m_{\tilde{\ell}}$ could produce much stronger suppression of σ^{SI} over a large range of m_χ (that is, not just in co-annihilation regions), the value of $m_{\tilde{\ell}} = 200$ GeV is already in significant tension with electron EDM constraints. Thus we conclude that the main effect of lower $m_{\tilde{\ell}}$ is to reduce the range of m_χ for which the χ can be the LSP, except perhaps for very low values $m_{\tilde{\ell}}$ which imply significant fine-tuning in CP phases.

Another well-motivated non-unified sfermion mass possibility is to have heavy first and second generation sfermions and light third generation sfermions. Precision measurements strongly constrain the mixing in the first two generations, but the mixing between the first two generations and the third generation is less well-constrained. An interesting possibility, then, is that the squarks of the first two generations are heavy to limit contributions to low-energy observables through decoupling, while the third generation squark masses are light to avoid fine-tuning in the electroweak scale [90–94]. The impact of such a sfermion mass pattern is shown in Fig. 7(b), which contrasts results for $\tilde{m} = 1$ TeV and the case where $m_{\tilde{t},\tilde{b}} = 500$ GeV, but all other sfermions remain at 1 TeV. Beyond lowering the upper limit on m_χ such that χ remains the LSP, a lower value for $m_{\tilde{t}}$ reduces the suppression of σ^{SI} associated with $t\bar{t}$ annihilation, as discussed in Sec. IV. There is also a slight widening of allowed values of σ^{SI} , as $\lambda_{b,t}$ do contribute to σ^{SI} , but this widening is not as significant as that caused by lowering \tilde{m} . Overall, the effect is larger than the effect of varying slepton masses, but again, it is not very significant.

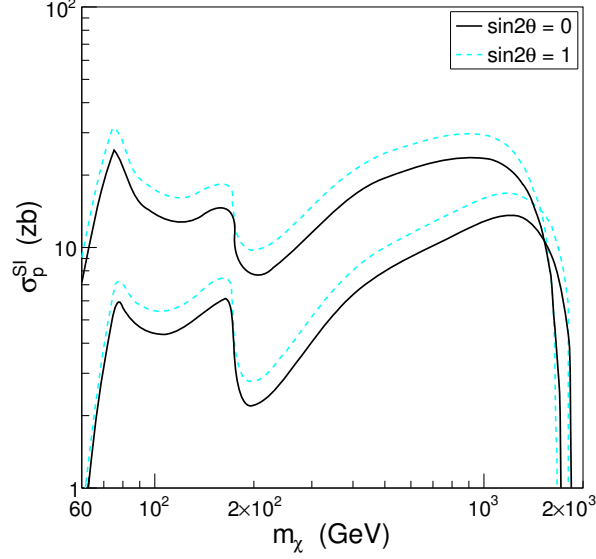


FIG. 8. *Dependence of σ^{SI} on left-right sfermion mixing.* Cross sections σ^{SI} are given for no left-right mixing and maximal left-right mixing for 3rd generation sfermions, $\mu > 0$ (upper) and $\mu < 0$ (lower), $\tilde{m} = 2$ TeV, $m_A = 4$ TeV, and $\tan \beta = 10$.

C. Left-Right Sfermion Mixing

Although we have assumed negligible left-right sfermion mixing, there may in general be some mixing, and this will alter both $\chi\chi$ annihilation through the process of Fig. 1(e) and σ^{SI} through the process of Fig. 3(c). Even if left-right mixing is only significant for third-generation sfermions, as is typically true, in principle this may affect σ^{SI} by modifying $\chi\chi$ annihilation in the early Universe or by changing the heavy quark contributions to scattering off nucleons.

Figure 8 shows the effect on σ^{SI} of left-right mixing in third generation sfermions. The mixing here is parameterized by the angle $\theta_{\tilde{q}}$, and the two cases shown are those with no mixing ($\sin 2\theta_{\tilde{q}} = 0$) and maximal mixing ($\sin 2\theta_{\tilde{q}} = 1$), for which each mass eigenstate has equal parts \tilde{f}_L and \tilde{f}_R . These are achieved by fixing the $A_{t,b,\tau}$ parameters appropriately. Although the latter case does produce some splitting between the \tilde{f} mass eigenstates, for the degenerate masses considered here, a highly mixed scenario can be achieved without a kinematically significant splitting for our analysis.⁶

As seen in Fig. 8, for $\tilde{m} = 2$ TeV, left-right mixing may enhance σ^{SI} by $\sim 15\%$. The effects of left-right mixing on the relic density calculation are minimal, but contributions from $\tilde{B}q_{L,R} \rightarrow \tilde{B}q_{R,L}$ and $\tilde{H}q_{L,R} \rightarrow \tilde{H}q_{R,L}$ produce an enhancement in σ^{SI} directly. The effect may be larger for lower \tilde{m} , but in any case, we find that the overall effect does not significantly impact conclusions about the characteristic range of σ^{SI} . The value of σ^{SI} is enhanced as χ becomes pure \tilde{H} at high mass by a process similar to Fig. 3(c) with \tilde{H} initial and final states, but this process is yukawa suppressed and σ^{SI} still drops below 1 zb in the highly \tilde{H} region.

⁶ The masses are not exactly degenerate, given corrections from D -terms, but even including these, a pair of completely mixed states can be created with a mass splitting of $\lesssim 2 - 3$ GeV for the values of \tilde{m} considered. These corrections are kept even in the no mixing case to prevent unintentional left-right mixing from numerical effects.

D. Explicit Inclusion of CP-Violation

Although the desire for $\mathcal{O}(1)$ CP-violating phases motivates large sfermion masses, we have performed our analysis in a manifestly CP-conserving framework. This is a cause for some concern, as CP violation could impact relic density and scattering calculations, which could, in principle, suppress σ^{SI} . In our model framework all CP violation is found in the phases of the parameters M_1 and μ . We adopt a convention where all CP violation is contained in the phase of the μ parameter ϕ_μ .

The effects of general phases on both Ω and σ^{SI} were discussed by the authors of Ref. [95], who found that phases can significantly enhance the relic density and suppress σ^{SI} . (See also Ref. [96].) For a highly-mixed neutralino LSP like the case considered here, varying the phase causes a suppression in both annihilation and scattering cross sections, leading to an enhancement in the relic density by a factor of ~ 5 and a suppression in σ^{SI} by a factor of ~ 50 . However, in that analysis the Ω_χ and σ^{SI} were treated as two independent parameters. In our analysis, with an appropriate relic density applied as a constraint, these effects tend to cancel each other: to achieve a viable relic density, $a_{\tilde{H}}$ must be increased to enhance annihilation, which will in turn enhance σ^{SI} .

To determine the effect, we note that the relic density is nearly minimal for $\phi_\mu = 0$ and maximal for $\phi_\mu = \pi$, with intermediate values for ϕ_μ smoothly interpolating between these two limits. The value of σ^{SI} has opposite behavior, with a maximal value for $\phi_\mu = 0$ and minimal value for $\phi_\mu = \pi$. The two limiting cases are, then, precisely the cases $\mu > 0$ and $\mu < 0$ that we have considered throughout our analysis. Thus the inclusion of an arbitrary CP-violating parameter should result in a simple interpolation between the cases of $\mu > 0$ and $\mu < 0$ as alluded to in Sec. V, without resulting in values of σ^{SI} outside of this range, except perhaps in finely-tuned portions of parameter space.

E. Strange Quark Content of the Nucleon

As discussed in Sec. IV, the value of σ^{SI} is strongly dependent on the individual quark contributions to the nucleon, f_q^N . Of these, the quantity that has traditionally had the most uncertainty is f_s^N , with quoted values ranging from 0.05 to 0.23. Recent lattice results suggest the lower value, and we have used this value throughout, but it is useful to examine the variation of σ^{SI} as f_s^N is varied. Throughout this section we use the assumption $f_q^p \approx f_q^n$.

To understand the general dependence on f_s^N , consider the quantity

$$f_{\text{tot}}^N = \sum_{q=1}^6 f_q^N, \quad (36)$$

which can be interpreted as the total quark contribution to the nucleon mass. The (perhaps unreasonably) high value $f_s^N = 0.23$ implies $f_{\text{tot}}^N \simeq 0.44$, and the low value $f_s^N = 0.05$ implies $f_{\text{tot}}^N \simeq 0.30$. Since f_Q^N is largely unchanged as f_s^N decreases further, even the unrealistic case of $f_s^N = 0$ would still have $f_{\text{tot}}^N \approx 0.25$. Thus, without considering further possible cancellations, the difference in σ^{SI} between no strange quark contribution to the nucleon and the largest proposed value should be about $(0.44/0.25)^2 \approx 3$. A more careful variation is shown in Fig. 9 for $\tilde{m} = 2$ TeV and 300 GeV. The 2 TeV case matches the sketched analysis above quite well — the value of σ^{SI} for $f_s^N = 0.05$ is suppressed by ~ 2

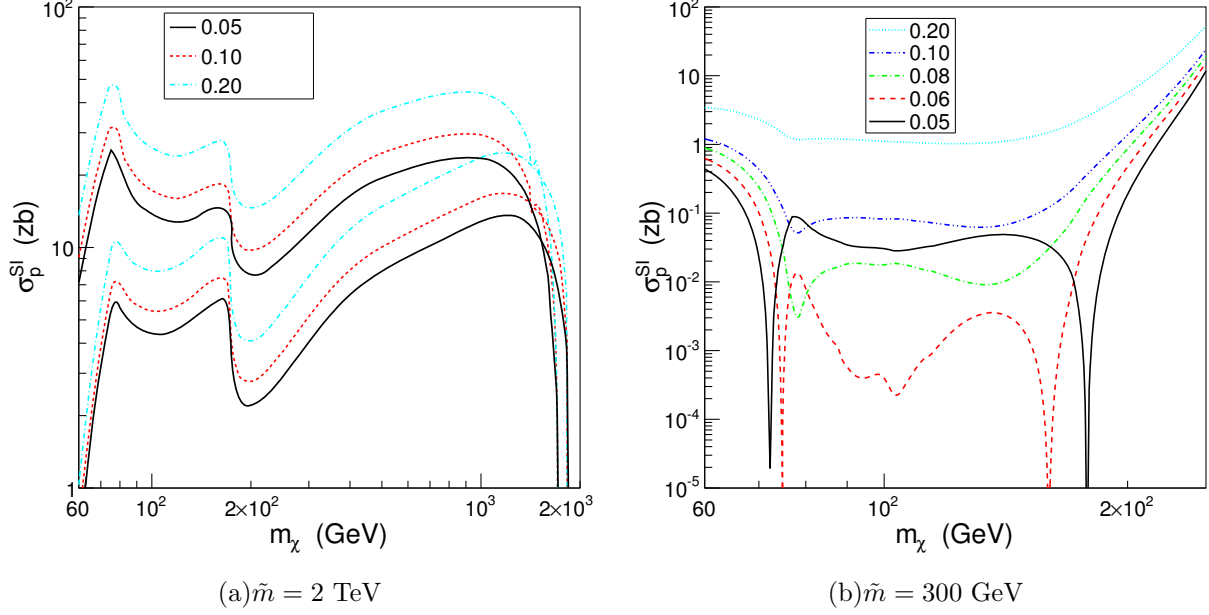


FIG. 9. Dependence of σ^{SI} on the strange quark content of the nucleon. Cross sections are given for the different values of f_s^p indicated, $m_A = 4$ TeV, and $\tan \beta = 10$. In panel (a), $\tilde{m} = 2$ TeV and $\mu > 0$ (upper) and $\mu < 0$ (lower). In panel (b), $\tilde{m} = 300$ GeV, and only the $\mu < 0$ curves are shown, as the $\mu > 0$ curves have much the same behavior as in panel (a).

relative to the value for $f_s^N = 0.2$, with the value for $f_s^N = 0.1$ lying in between, in good agreement with the prediction based on f_{tot}^N . Note that, for $\tilde{m} = 2$ TeV, our default value of f_s^N yields the lowest σ^{SI} , and other possible values imply improved prospects for direct detection.

For $\tilde{m} = 300$ GeV the suppression for low f_s^N is much more pronounced, at least in the case of $\mu < 0$. As discussed in Sec. IV, for $\mu < 0$ the sfermion contribution to scattering is similar in size to the Higgs contribution, opening the possibility of cancellation regardless of the value of m_χ . In fact, this also opens up the possibility for additional cancellations between λ_q for different quarks based on relative values of f_q^p . The cancellation is most prominent when f_s^N is comparable to the contributions of other quarks; for larger values of f_s^N the strange quark is the dominant contribution to nucleon mass, which raises the generic value of σ^{SI} . Even for larger f_s^N , however, σ^{SI} for $\tilde{m} = 300$ GeV remains suppressed relative to higher values of \tilde{m} due to the squark-Higgs contribution cancellations discussed in Sec. IV.

F. Variations in Relic Density

It is possible that neutralinos form some, but not all, of the dark matter. One may consider models with $\Omega_\chi < 0.23$, which may have larger σ^{SI} . Of course the direct detection signal is proportional not to σ^{SI} , but to $\Omega_\chi \sigma^{SI}$. In fact, as is well-known, for thermal relics, the relic density is inversely proportional to $\langle \sigma_{\text{an}} v \rangle$, the thermally-averaged annihilation cross section. If σ^{SI} and σ_{an} scale together, then the gain in σ^{SI} is exactly compensated by the reduction in Ω_χ .

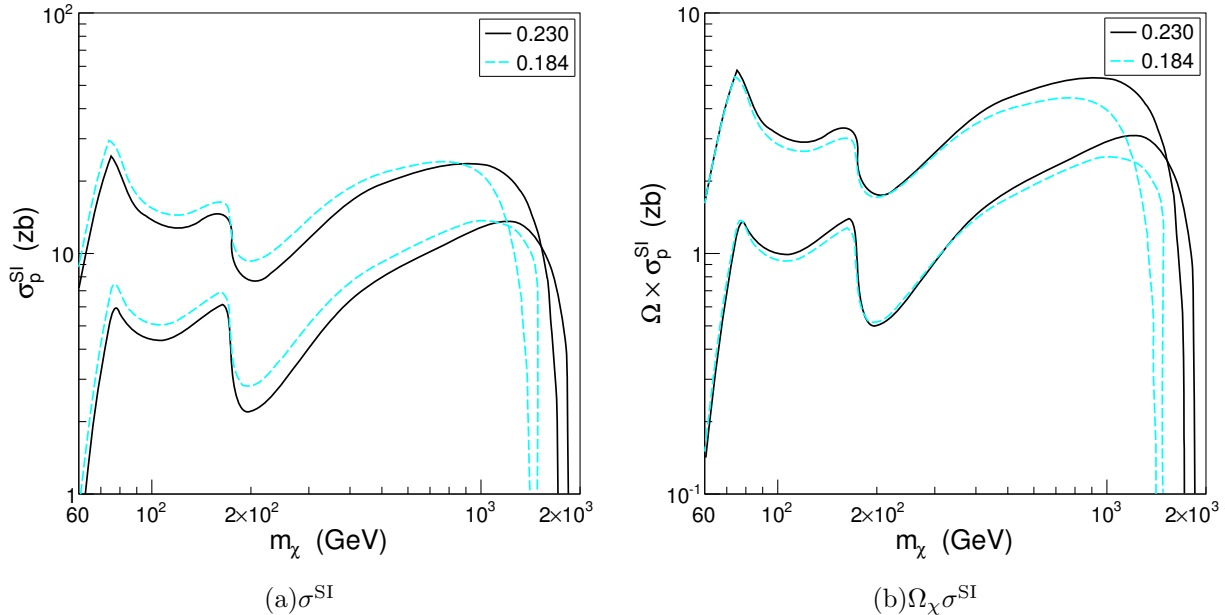


FIG. 10. *Dependence of σ^{SI} on Ω_χ .* Cross sections σ^{SI} are given for the values of Ω_χ indicated, $\mu > 0$ (upper) and $\mu < 0$ (lower), $\tilde{m} = 2$ TeV, $m_A = 4$ TeV, and $\tan \beta = 10$.

In Fig. 10, we explore the impact of variations in Ω_χ . For concreteness, we consider models with $\Omega_\chi = 0.184$. As expected, in Fig. 10(a), we see that these models have larger σ^{SI} . However, in Fig. 10(b), we see that this is almost exactly compensated by the reduction in Ω_χ except at high m_χ , leaving the direct detection signal invariant. At very high m_χ , the neutralino becomes nearly pure \tilde{H} and reaches its maximum annihilation efficiency more quickly for the lower value of Ω . For relatively small deviations from the assumption $\Omega_\chi = 0.23$, then, the direct detection signal is not impacted by the exact value of Ω_χ assumed except for large m_χ . This result may not hold for large deviations when χ constitutes a very small portion of the dark matter, but in this case the theoretical motivation for χ dark matter is somewhat strained.

G. Galactic Small-Scale Structure

The exclusion limits on σ^{SI} are also affected by the local density of DM. Although a naïve approximation suggests a spherical DM halo with uniform density at a given radius, small scale structure exists, and leads to a few regions with higher than average density, compensated for by a lower than average density in the rest of the space. This has been studied in Ref. [97], which concluded that while the reduction in general number density from clumping might be as much as an order of magnitude, the more likely possibility is a reduction by less than a factor of two. This implies that experimental limits are subject to astrophysical uncertainties, but does not significantly alter our conclusion that near future experiments will probe the heart of neutralino parameter space.

H. Extension to Non-minimal Scenarios

Because we work in a manifestly low-energy framework, our results can easily be generalized beyond the MSSM to models that include new superfields with TeV-scale masses. Although such fields will in general affect the annihilation and scattering of χ dark matter, we argue that σ^{SI} remains generically in the range $1 \text{ zb} \lesssim \sigma^{\text{SI}} \lesssim 40 \text{ zb}$.

To illustrate this point, consider first the impact of a new TeV-scale particle X on annihilation. Assume that X couples to χ and some set of other MSSM particles with a coupling of order α_W . The effect of X will be most pronounced if there is resonant annihilation when $m_X \approx 2m_\chi$ or if there is significant co-annihilation when $m_X \approx m_\chi$. Both cases force a severe suppression in $a_{\tilde{H}}$ to compensate and produce a sufficiently large relic density⁷, in turn causing a large suppression in σ^{SI} similar to that seen in the h and A resonances discussed above. However, outside of these fine-tuned regions of parameter space, new X -mediated processes must be roughly the same size as existing processes to be relevant and will generally decrease (or possibly increase in the case of cancellation) $a_{\tilde{H}}$ relative to the MSSM case. Although this will produce a suppression (or possibly enhancement) of σ^{SI} , the additional effect should not generically be greater than the factor of $2 - 3$ that is caused by the introduction of W^+W^- or $t\bar{t}$ annihilation.

In scattering, if X couples to quarks, it may induce additional contributions to σ^{SI} . However, although the mass and interactions of X may be chosen to significantly suppress σ^{SI} , such an effect requires a fine-tuning of the mass and couplings of X to produce a cancellation similar to the case of $\tilde{m} = 300 \text{ GeV}$ discussed in Sec. IV. Indeed, the low value of m_X required to cause a severe suppression directly through scattering effects should naïvely interfere with low-energy observables due to its couplings to quarks, and such operators are constrained by collider searches [29–31]. Even if constraints on the mass of X can be avoided by tuning couplings, a sufficiently light mass for X places it generically within detection reach of the LHC.

VII. SPIN-DEPENDENT CROSS SECTIONS

We have focused in this work on spin-independent direct detection, as this provides bright prospects for the discovery of neutralino dark matter. It is interesting, nonetheless, to examine the prospects for spin-dependent cross sections, which is probed both by direct detection experiments, and by indirect detection searches for neutrinos.

Spin-dependent scattering proceeds through the effective operator

$$\alpha_i \bar{\chi} \gamma^\mu \gamma^5 \chi \bar{q}_i \gamma_\mu \gamma^5 q_i . \quad (37)$$

The structure of these operators implies that the contributing diagrams will be similar to those shown in Fig. 3, except with Z -mediated scattering replacing Higgs-mediated scattering, and the replacement $\tilde{B} \leftrightarrow \tilde{H}$ and associated fermion $L \leftrightarrow R$ replacements on one leg in

⁷ If reducing $a_{\tilde{H}}$ does not compensate for the resonant annihilation, then that region will generally not provide a viable relic density.

both Fig. 3(b) and Fig. 3(c). The associated coefficients have the form [85]

$$\alpha_u = \frac{g^2}{2(m_{\tilde{u}_i}^2 - m_\chi^2)} \left[\left| \left(\frac{1}{2} a_{\tilde{W}} + \frac{1}{6} \tan \theta_W a_{\tilde{B}} \right) U_{i1}^{(\tilde{u})*} + \frac{m_u a_{\tilde{H}_u}}{2m_W \sin \beta} U_{i2}^{(\tilde{u})*} \right|^2 \right. \\ \left. + \left| \frac{m_u a_{\tilde{H}_u}}{2m_W \sin \beta} U_{i1}^{(\tilde{u})} - \frac{2}{3} \tan \theta_W a_{\tilde{B}} U_{i2}^{(\tilde{u})} \right|^2 \right] \\ - \frac{g^2}{8m_Z^2 \cos^2 \theta_W} (|a_{\tilde{H}_d}|^2 - |a_{\tilde{H}_u}|^2) \quad (38)$$

$$\alpha_d = \frac{g^2}{2(m_{\tilde{d}_i}^2 - m_\chi^2)} \left[\left| \left(-\frac{1}{2} a_{\tilde{W}} + \frac{1}{6} \tan \theta_W a_{\tilde{B}} \right) U_{i1}^{(\tilde{d})*} + \frac{m_d a_{\tilde{H}_d}}{2m_W \cos \beta} U_{i2}^{(\tilde{d})*} \right|^2 \right. \\ \left. + \left| \frac{m_d a_{\tilde{H}_d}}{2m_W \cos \beta} U_{i1}^{(\tilde{d})} + \frac{1}{3} \tan \theta_W a_{\tilde{B}} U_{i2}^{(\tilde{d})} \right|^2 \right] \\ + \frac{g^2}{8m_Z^2 \cos^2 \theta_W} (|a_{\tilde{H}_d}|^2 - |a_{\tilde{H}_u}|^2) , \quad (39)$$

with the same notation used in Sec. IV B.

The spin-dependent couplings will exhibit a similar suppression of sfermion-mediated diagrams relative to Z -mediated diagrams as seen in the spin-independent case, with the smaller value of m_Z relative to m_h leading to the naïve expectation that the squark mass necessary to cause serious suppression should be lower than the 300 GeV mass necessary to suppress σ^{SI} . Such a small mass is ruled out by collider bounds. Moreover, as long as $a_{\tilde{H}_{u,d}}$ are non-negligible, the squark-mediated contribution to the cross section suffers an additional suppression relative to the Z -mediated contribution of

$$\sim \sin^4 \theta_W \left(\frac{|a_{\tilde{B}}|^2}{|a_{\tilde{H}_d}|^2 - |a_{\tilde{H}_u}|^2} \right)^2 , \quad (40)$$

in contrast to the minor suppression of the Higgs-mediated contribution relative to the squark-mediated contribution due to the mixing angle α for σ^{SI} .

Predictions for σ^{SD} for neutralino-proton scattering are given in Fig. 11, using the same parameters as in Sec. V and three values of \tilde{m} . In all three cases, the dominant effect is a drop in σ^{SD} with increasing m_χ . This is due to the proportionality of the Z -mediated contribution to the factor $|a_{\tilde{H}_d}|^2 - |a_{\tilde{H}_u}|^2$; as demonstrated in Fig. 2(a), the values of $|a_{\tilde{H}_{u,d}}|$ converge with increasing m_χ , thus suppressing σ^{SD} . The dependence on \tilde{m} is mild until higher values of m_χ where the Z -mediated contribution is self-suppressed to the level of the sfermion-mediated contribution, and even the differences in σ^{SD} at $m_\chi < 100$ GeV are due to the slight variation in $a_{\tilde{H}}$ with mass shown in Fig. 2(b) rather than cancellations between scattering processes.

The limits plotted in Fig. 11 correspond to upper limits on σ^{SD} from the AMANDA [98] and IceCube [99] experiments, along with projected upper limits from a 10 year run of IceCube with DeepCore, an extension of IceCube with tighter string and optical module spacing [100] and a 4 kg COUPP, assumed to run background free for 3 months at a deep underground site [101]. The entire characteristic region plotted lies outside current upper limits, but the projected IceCube limits intersect the allowed region for $60 \text{ GeV} \lesssim m_\chi \lesssim$

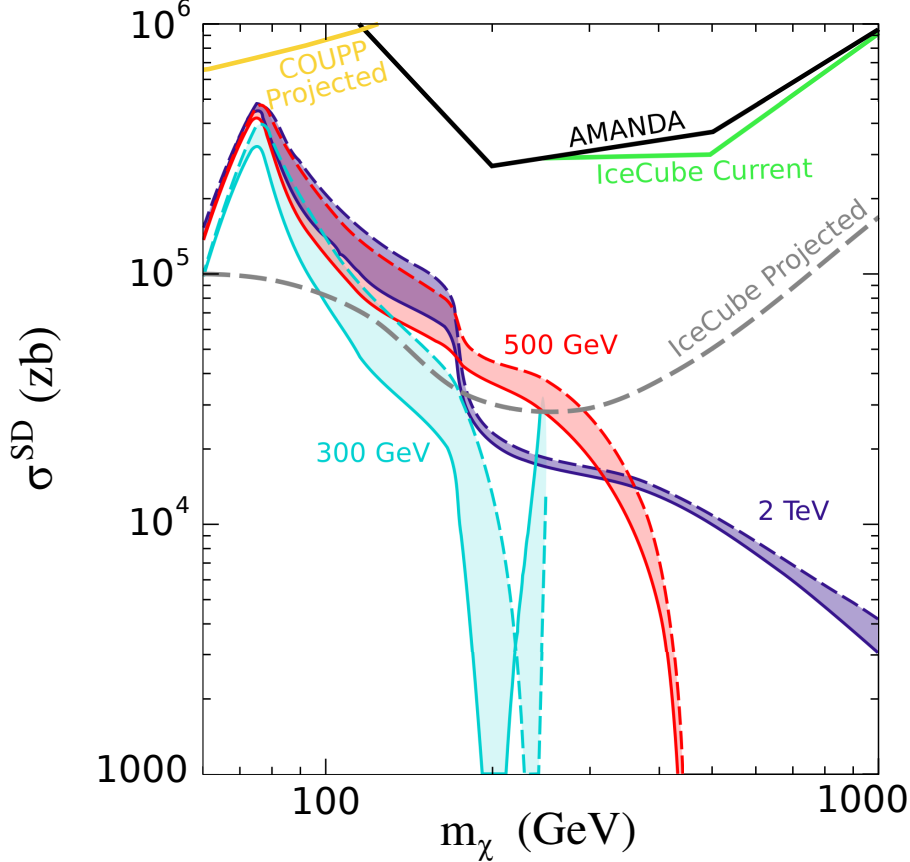


FIG. 11. Characteristic values for spin-dependent neutralino-proton scattering cross sections σ^{SD} . The shaded regions are σ^{SD} for the values \tilde{m} indicated, with $\mu > 0$ (solid border) and $\mu < 0$ (dashed border), $m_A = 4$ TeV, and $\tan \beta = 10$. Also shown are current limits from the AMANDA [98] and IceCube [99] experiments, and the projected sensitivities of a 10-year run of IceCube with DeepCore [100] and a 4kg COUPP running at a deep underground site [101].

200 GeV for most values of \tilde{m} , and the $\tilde{m} = 500$ GeV region may be within IceCube's sensitivity region up to $m_\chi \sim 300$ GeV.

We conclude that, at least for the neutralino DM models considered here, spin-dependent searches are indeed not as promising as spin-independent searches in the near future. However, for some parts of parameter space, spin-dependent searches may also see a signal in the coming years. Of course, if a signal is seen in spin-independent detection, confirmation through spin-dependent signals will be an essential supplement.

VIII. CONCLUSIONS

Experimental sensitivities to the scattering of dark matter off normal matter are improving rapidly. In this study, we have addressed the question of what this progress implies for the discovery prospects for neutralino dark matter. To determine characteristic spin-independent and spin-dependent neutralino-nucleon cross sections, we have worked not with specific high-energy models, but rather in a phenomenological framework incorporating only the basic motivations for SUSY (the gauge hierarchy problem, force unification, and the

WIMP miracle) and experimental constraints (direct searches and bounds on flavor and CP violation).

SUSY parameter space is large and complicated, but our strategy has been to start in a simple corner and work out from there. The conclusions of this study may be summarized as follows. We assume gaugino mass unification, as motivated by gauge coupling unification, and, to begin with, also heavy squarks and sleptons, as motivated by stringent constraints on flavor and CP violation. All of neutralino dark matter phenomenology then depends only on the Bino and Higgsino mass parameters M_1 and μ , and the heavy Higgs scalar mass m_A and $\tan\beta$. Away from Higgs resonances, the dependence on the latter two parameters is weak. Requiring the correct thermal relic density removes another degree of freedom, leaving only one, which may be taken to be the neutralino mass m_χ . For $m_\chi \gtrsim 70$ GeV, the spin-independent cross section lies in the range $1 \text{ zb} \lesssim \sigma^{\text{SI}} \lesssim 40 \text{ zb}$ and is highly insensitive to m_χ for the reasons detailed above. The assumption of a unified sfermion mass disregards the complicated spectrum details associated with any high-scale model, but according to the discussion above such effects should be sub-dominant in any case except in very special cases such as co-annihilation. While the mass splittings of full spectra would certainly alter a specific prediction for σ^{SI} , such effects will not alter the *characteristic* value of σ^{SI} studied here.

From this result, we then generalize to other regions of parameter space. Surprisingly, the upper and lower limits of the characteristic range only vary by factors of ~ 2 for sfermion masses as low as $\tilde{m} \sim 400$ GeV. For very light sfermions near their experimental bound $\tilde{m} \sim 300$ GeV, large cancellations between contributions from up- and down-type quarks are possible. We have also identified and analyzed two other fine-tuned scenarios with greatly reduced σ^{SI} , where annihilation is enhanced either by resonances when $2m_\chi \approx m_h$ or m_A or by co-annihilation when $m_\chi \approx \tilde{m}$. In these special cases, σ^{SI} falls outside our characteristic range.

We next considered the effects of un-unifying the slepton and squark masses, un-unifying the third generation squark masses, including significant left-right sfermion mixing, and including CP-violating phases in the relic density and σ^{SI} calculations. In each of these cases, for fixed Ω_χ , we find typically small variations in the allowed range of σ^{SI} . We have also explored variations of the strange quark content of the nucleon and found that our assumed value of $f_s^N = 0.05$ is conservative, with other values enhancing σ^{SI} for $\tilde{m} \gtrsim 400$ GeV. Finally, we also considered the possibility of multi-component dark matter where neutralinos are just one significant component. In this case, neutralino annihilation must be enhanced to reduce the thermal relic density, but this also enhances σ^{SI} . These effects effectively cancel, leaving the experimental direct detection signal, which is proportional to $\Omega_\chi \sigma^{\text{SI}}$, invariant and in our characteristic range.

These results for σ^{SI} are compared to experiment in Fig. 5. If dark matter is composed of thermal relic neutralinos, the prospects for near future experiments that are sensitive to the zeptobarn scale are truly promising. We have also analyzed the prospects for spin-dependent scattering. These are summarized in Fig. 11. Although not as promising as spin-independent scattering, observable signals exist for dark matter masses $m_\chi \lesssim 500$ GeV.

Our results are complementary to those based on high-energy frameworks. In the context of mSUGRA, for example, the fine-tuned possibilities of resonant annihilation and co-annihilation also exist and are known to predict low σ^{SI} . This results of this study show that these phenomena are decoupled from other SUSY phenomenology typically related to them in mSUGRA. For example, the A resonance may be realized at any $\tan\beta$, as opposed

to only high $\tan\beta$ in mSUGRA. Nevertheless, these possibilities remain fine-tuned, in the sense of requiring specific relations between superpartner masses that are not suggested by experimental constraints or foundational motivations of SUSY.

At the same time, this study shows that results from the focus point region of mSUGRA are robust. As is well-known, in the focus point region, the neutralino is a well-mixed Bino-Higgsino combination and, for this reason, rates for both direct and indirect detection are large, with predictions for spin-independent cross sections in the range $\sigma^{\text{SI}} \sim 1 - 10$ zb. The results of this study show that similar cross sections are achieved in a more general setting throughout parameter space, largely independent of assumptions about GUT boundary conditions, A parameters, $\tan\beta$, or even the details of the slepton and squark spectra, provided $\tilde{m} \gtrsim 400$ GeV. Large direct detection signals and light sfermions are therefore perfectly consistent, with positive implications for both dark matter experiments and colliders. Given the generality of our model framework, the results for characteristic σ^{SI} will apply to a diverse array of high-energy models.

In conclusion, the field is reaching a critical juncture in the search for neutralino dark matter. We have identified a range for characteristic cross sections for neutralino-nucleon scattering. These are by no means a lower limit on possible value of σ^{SI} ; indeed several possibilities for much smaller cross-sections were identified in this work. Nevertheless, even in the most pessimistic scenario, the identification of a characteristic cross section range has important consequences. If no signal is seen at the zeptobarn scale, then a model with thermal relic neutralinos must contain some amount of fine-tuning. This could be accomplished by enhanced annihilation through resonances or co-annihilation, as noted above. Alternatively, one could introduce new particles that induce neutralino-quark couplings that cancel existing contributions to σ^{SI} . As we have seen, however, the scale of existing contributions is set by the light Higgs boson mass m_h , not by a superpartner mass. These new contributions would typically be associated with light, colored fields, then, as in the case of the ~ 300 GeV squarks we discussed in detail, and would be within reach of collider experiments.

Of course, the most straightforward and natural conclusion is that if thermal relic neutralinos are a significant component of dark matter, their spin-independent scattering cross section likely lies in the range $1 \text{ zb} \lesssim \sigma^{\text{SI}} \lesssim 40 \text{ zb}$, just beyond current sensitivities. Current and near future experiments will therefore see a signal as they probe down to the zeptobarn scale, and the next generation of experiments will compile the statistics required to definitively establish the signal on different targets, constrain the dark matter's mass, see signals in directional detectors, and usher in the era of dark matter astronomy.

ACKNOWLEDGMENTS

We are grateful to Jeff Filippini, Konstantin Matchev, Will Shepherd, Hank Sobel, Tim Tait, and Xerxes Tata for helpful correspondence and conversations. This work was supported in part by NSF grants PHY-0653656 and PHY-0970173.

-
- [1] G. Bertone, D. Hooper, and J. Silk, “Particle dark matter: Evidence, candidates and constraints,” *Phys. Rept.* **405** (2005) 279–390, [arXiv:hep-ph/0404175](#).

- [2] L. Bergstrom, “Dark Matter Candidates,” *New J. Phys.* **11** (2009) 105006, [arXiv:0903.4849 \[hep-ph\]](#).
- [3] J. L. Feng, “Dark Matter Candidates from Particle Physics and Methods of Detection,” *Ann. Rev. Astron. Astrophys.* **48** (2010) 495–545, [arXiv:1003.0904 \[astro-ph.CO\]](#).
- [4] R. Bernabei *et al.*, “New results from DAMA/LIBRA,” *Eur. Phys. J.* **C67** (2010) 39–49, [arXiv:1002.1028 \[astro-ph.GA\]](#).
- [5] **XENON10** Collaboration, J. Angle *et al.*, “Limits on spin-dependent WIMP-nucleon cross-sections from the XENON10 experiment,” *Phys. Rev. Lett.* **101** (2008) 091301, [arXiv:0805.2939 \[astro-ph\]](#).
- [6] **The CDMS-II** Collaboration, Z. Ahmed *et al.*, “Dark Matter Search Results from the CDMS II Experiment,” *Science* **327** (2010) 1619–1621, [arXiv:0912.3592 \[astro-ph.CO\]](#).
- [7] **CoGeNT** Collaboration, C. E. Aalseth *et al.*, “Results from a Search for Light-Mass Dark Matter with a P- type Point Contact Germanium Detector,” [arXiv:1002.4703 \[astro-ph.CO\]](#).
- [8] **XENON100** Collaboration, E. Aprile *et al.*, “First Dark Matter Results from the XENON100 Experiment,” [arXiv:1005.0380 \[astro-ph.CO\]](#).
- [9] **XENON100** Collaboration, E. Aprile *et al.*, “Likelihood Approach to the First Dark Matter Results from XENON100,” [arXiv:1103.0303 \[hep-ex\]](#).
- [10] **XENON100** Collaboration, E. Aprile *et al.*, “Dark Matter Results from 100 Live Days of XENON100 Data,” [arXiv:1104.2549 \[astro-ph.CO\]](#).
- [11] **XENON100** Collaboration, E. Aprile, L. Baudis, *et al.*, “Status and Sensitivity Projections for the XENON100 Dark Matter Experiment,” *PoS IDM2008* (2008) 018, [arXiv:0902.4253 \[astro-ph.IM\]](#).
- [12] **CRESST** Collaboration, J. Schmalzer *et al.*, “Status of the CRESST Dark Matter Search,” [arXiv:0912.3689 \[astro-ph.IM\]](#).
- [13] **LUX** Collaboration, D. N. McKinsey *et al.*, “The LUX dark matter search,” *J. Phys. Conf. Ser.* **203** (2010) 012026.
- [14] **XMASS** Collaboration, H. Sekiya *et al.*, “XMASS,” [arXiv:1006.1473 \[astro-ph.IM\]](#).
- [15] **DEAP/CLEAN** Collaboration, A. Hime, “DEAP & CLEAN detectors for low energy particle astrophysics,” *AIP Conf. Proc.* **870** (2006) 205–207.
- [16] **WArP** Collaboration, R. Acciarri *et al.*, “The WArP experiment,” *J. Phys. Conf. Ser.* **203** (2010) 012006.
- [17] T. Bruch and f. t. C. Collaboration, “CDMS-II to SuperCDMS: WIMP search at a zeptobarn,” [arXiv:1001.3037 \[astro-ph.IM\]](#).
- [18] L. E. Strigari, “Neutrino Coherent Scattering Rates at Direct Dark Matter Detectors,” *New J. Phys.* **11** (2009) 105011, [arXiv:0903.3630 \[astro-ph.CO\]](#).
- [19] A. Gutlein *et al.*, “Solar and Atmospheric Neutrinos: Background Sources for the Direct Dark Matter Searches,” *Astropart. Phys.* **34** (2010) 90–96, [arXiv:1003.5530 \[hep-ph\]](#).
- [20] H. Goldberg, “Constraint on the photino mass from cosmology,” *Phys. Rev. Lett.* **50** (1983) 1419.
- [21] J. R. Ellis, J. S. Hagelin, D. V. Nanopoulos, K. A. Olive, and M. Srednicki, “Supersymmetric relics from the big bang,” *Nucl. Phys.* **B238** (1984) 453–476.
- [22] M. Drees and M. M. Nojiri, “The Neutralino relic density in minimal $N = 1$ supergravity,” *Phys. Rev.* **D47** (1993) 376–408, [arXiv:hep-ph/9207234](#).
- [23] M. Drees and M. Nojiri, “Neutralino-Nucleon Scattering Revisited,” *Phys. Rev.* **D48** (1993) 3483–3501, [arXiv:hep-ph/9307208](#).

- [24] G. Jungman, M. Kamionkowski, and K. Griest, “Supersymmetric dark matter,” *Phys. Rept.* **267** (1996) 195–373, [arXiv:hep-ph/9506380](#).
- [25] A. Bottino, F. Donato, N. Fornengo, and S. Scopel, “Interpreting the recent results on direct search for dark matter particles in terms of relic neutralino,” *Phys. Rev.* **D78** (2008) 083520, [arXiv:0806.4099 \[hep-ph\]](#).
- [26] D. Feldman, Z. Liu, and P. Nath, “Low Mass Neutralino Dark Matter in the MSSM with Constraints from $B_s \rightarrow \mu^+ \mu^-$ and Higgs Search Limits,” *Phys. Rev.* **D81** (2010) 117701, [arXiv:1003.0437 \[hep-ph\]](#).
- [27] E. Kuflik, A. Pierce, and K. M. Zurek, “Light Neutralinos with Large Scattering Cross Sections in the Minimal Supersymmetric Standard Model,” *Phys. Rev.* **D81** (2010) 111701, [arXiv:1003.0682 \[hep-ph\]](#).
- [28] V. Mandic, A. Pierce, P. Gondolo, and H. Murayama, “The Lower bound on the neutralino nucleon cross-section,” [arXiv:hep-ph/0008022](#).
- [29] J. Goodman *et al.*, “Constraints on Light Majorana Dark Matter from Colliders,” *Phys. Lett.* **B695** (2011) 185–188, [arXiv:1005.1286 \[hep-ph\]](#).
- [30] J. Goodman *et al.*, “Constraints on Dark Matter from Colliders,” *Phys. Rev.* **D82** (2010) 116010, [arXiv:1008.1783 \[hep-ph\]](#).
- [31] Y. Bai, P. J. Fox, and R. Harnik, “The Tevatron at the Frontier of Dark Matter Direct Detection,” *JHEP* **12** (2010) 048, [arXiv:1005.3797 \[hep-ph\]](#).
- [32] J. Fan, M. Reece, and L.-T. Wang, “Non-relativistic effective theory of dark matter direct detection,” *JCAP* **1011** (2010) 042, [arXiv:1008.1591 \[hep-ph\]](#).
- [33] A. H. Chamseddine, R. L. Arnowitt, and P. Nath, “Locally Supersymmetric Grand Unification,” *Phys. Rev. Lett.* **49** (1982) 970.
- [34] R. Barbieri, S. Ferrara, and C. A. Savoy, “Gauge Models with Spontaneously Broken Local Supersymmetry,” *Phys. Lett.* **B119** (1982) 343.
- [35] N. Ohta, “Grand unified theories based on local supersymmetry,” *Prog. Theor. Phys.* **70** (1983) 542.
- [36] L. J. Hall, J. D. Lykken, and S. Weinberg, “Supergravity as the Messenger of Supersymmetry Breaking,” *Phys. Rev.* **D27** (1983) 2359–2378.
- [37] L. Alvarez-Gaume, J. Polchinski, and M. B. Wise, “Minimal Low-Energy Supergravity,” *Nucl. Phys.* **B221** (1983) 495.
- [38] J. R. Ellis, T. Falk, K. A. Olive, and M. Srednicki, “Calculations of neutralino stau coannihilation channels and the cosmologically relevant region of MSSM parameter space,” *Astropart. Phys.* **13** (2000) 181–213, [arXiv:hep-ph/9905481](#).
- [39] H. Baer, C. Balazs, and A. Belyaev, “Neutralino relic density in minimal supergravity with co- annihilations,” *JHEP* **03** (2002) 042, [arXiv:hep-ph/0202076](#).
- [40] J. L. Feng, K. T. Matchev, and F. Wilczek, “Neutralino Dark Matter in Focus Point Supersymmetry,” *Phys. Lett.* **B482** (2000) 388–399, [arXiv:hep-ph/0004043](#).
- [41] J. L. Feng, K. T. Matchev, and F. Wilczek, “Prospects for indirect detection of neutralino dark matter,” *Phys. Rev.* **D63** (2001) 045024, [arXiv:astro-ph/0008115](#).
- [42] H. Baer, T. Krupovnickas, S. Profumo, and P. Ullio, “Model independent approach to focus point supersymmetry: From dark matter to collider searches,” *JHEP* **10** (2005) 020, [arXiv:hep-ph/0507282](#).
- [43] J. R. Ellis, T. Falk, G. Ganis, K. A. Olive, and M. Srednicki, “The CMSSM Parameter Space at Large $\tan \beta$,” *Phys. Lett.* **B510** (2001) 236–246, [arXiv:hep-ph/0102098](#).

- [44] R. R. de Austri, R. Trotta, and L. Roszkowski, “A Markov chain Monte Carlo analysis of the CMSSM,” *JHEP* **05** (2006) 002, [arXiv:hep-ph/0602028](#).
- [45] R. Trotta, R. R. de Austri, and L. Roszkowski, “Prospects for direct dark matter detection in the constrained MSSM,” *New Astron. Rev.* **51** (2007) 316–320, [arXiv:astro-ph/0609126](#).
- [46] R. Trotta, F. Feroz, M. P. Hobson, L. Roszkowski, and R. Ruiz de Austri, “The Impact of priors and observables on parameter inferences in the Constrained MSSM,” *JHEP* **12** (2008) 024, [arXiv:0809.3792 \[hep-ph\]](#).
- [47] H. Baer, A. Mustafayev, E.-K. Park, and X. Tata, “Target dark matter detection rates in models with a well-tempered neutralino,” *JCAP* **0701** (2007) 017, [arXiv:hep-ph/0611387](#).
- [48] **MSSM Working Group** Collaboration, A. Djouadi *et al.*, “The Minimal supersymmetric standard model: Group summary report,” [arXiv:hep-ph/9901246](#).
- [49] A. Djouadi, J.-L. Kneur, and G. Moultaka, “SuSpect: A Fortran code for the supersymmetric and Higgs particle spectrum in the MSSM,” *Comput. Phys. Commun.* **176** (2007) 426–455, [arXiv:hep-ph/0211331](#).
- [50] C. F. Berger, J. S. Gainer, J. L. Hewett, and T. G. Rizzo, “Supersymmetry Without Prejudice,” *JHEP* **02** (2009) 023, [arXiv:0812.0980 \[hep-ph\]](#).
- [51] R. C. Cotta, J. S. Gainer, J. L. Hewett, and T. G. Rizzo, “Dark Matter in the MSSM,” *New J. Phys.* **11** (2009) 105026, [arXiv:0903.4409 \[hep-ph\]](#).
- [52] B. C. Allanach, “SOFTSUSY: A C++ program for calculating supersymmetric spectra,” *Comput. Phys. Commun.* **143** (2002) 305–331, [arXiv:hep-ph/0104145](#).
- [53] G. Belanger, F. Boudjema, A. Pukhov, and A. Semenov, “micrOMEGAs2.0: A program to calculate the relic density of dark matter in a generic model,” *Comput. Phys. Commun.* **176** (2007) 367–382, [arXiv:hep-ph/0607059](#).
- [54] G. Belanger, F. Boudjema, A. Pukhov, and A. Semenov, “Dark matter direct detection rate in a generic model with micrOMEGAs2.1,” *Comput. Phys. Commun.* **180** (2009) 747–767, [arXiv:0803.2360 \[hep-ph\]](#).
- [55] S. Mizuta, D. Ng, and M. Yamaguchi, “Phenomenological aspects of supersymmetric standard models without grand unification,” *Phys. Lett.* **B300** (1993) 96–103, [arXiv:hep-ph/9210241](#).
- [56] H. Baer, A. Mustafayev, E.-K. Park, S. Profumo, and X. Tata, “Mixed higgsino dark matter from a reduced SU(3) gaugino mass: Consequences for dark matter and collider searches,” *JHEP* **04** (2006) 041, [arXiv:hep-ph/0603197](#).
- [57] H. Baer, A. Mustafayev, H. Summy, and X. Tata, “Mixed Higgsino Dark Matter from a Large SU(2) Gaugino Mass,” *JHEP* **10** (2007) 088, [arXiv:0708.4003 \[hep-ph\]](#).
- [58] G. Anderson *et al.*, “Motivations for and implications of non-universal GUT- scale boundary conditions for soft SUSY-breaking parameters,” [arXiv:hep-ph/9609457](#).
- [59] U. Chattopadhyay, A. Corsetti, and P. Nath, “Supersymmetric dark matter and Yukawa unification,” *Phys. Rev.* **D66** (2002) 035003, [arXiv:hep-ph/0201001](#).
- [60] J. R. Ellis, K. A. Olive, and Y. Santoso, “The MSSM Parameter Space with Non-Universal Higgs Masses,” *Phys. Lett.* **B539** (2002) 107–118, [arXiv:hep-ph/0204192](#).
- [61] A. Birkedal-Hansen and B. D. Nelson, “Relic neutralino densities and detection rates with nonuniversal gaugino masses,” *Phys. Rev.* **D67** (2003) 095006, [arXiv:hep-ph/0211071](#).
- [62] J. R. Ellis, A. Ferstl, K. A. Olive, and Y. Santoso, “Direct Detection of Dark Matter in the MSSM with Non- Universal Higgs Masses,” *Phys. Rev.* **D67** (2003) 123502, [arXiv:hep-ph/0302032](#).

- [63] H. Baer, A. Mustafayev, S. Profumo, A. Belyaev, and X. Tata, “Direct, indirect and collider detection of neutralino dark matter in SUSY models with non-universal Higgs masses,” *JHEP* **07** (2005) 065, [arXiv:hep-ph/0504001](#).
- [64] J. L. Feng, K. T. Matchev, and Y. Shadmi, “Theoretical Expectations for the Muon’s Electric Dipole Moment,” *Nucl. Phys.* **B613** (2001) 366–381, [arXiv:hep-ph/0107182](#).
- [65] T. Moroi, “The Muon Anomalous Magnetic Dipole Moment in the Minimal Supersymmetric Standard Model,” *Phys. Rev.* **D53** (1996) 6565–6575, [arXiv:hep-ph/9512396](#).
- [66] B. C. Regan, E. D. Commins, C. J. Schmidt, and D. DeMille, “New limit on the electron electric dipole moment,” *Phys. Rev. Lett.* **88** (2002) 071805.
- [67] C. A. Baker *et al.*, “An improved experimental limit on the electric dipole moment of the neutron,” *Phys. Rev. Lett.* **97** (2006) 131801, [arXiv:hep-ex/0602020](#).
- [68] **Muon G-2** Collaboration, G. W. Bennett *et al.*, “Final report of the muon E821 anomalous magnetic moment measurement at BNL,” *Phys. Rev.* **D73** (2006) 072003, [arXiv:hep-ex/0602035](#).
- [69] **Heavy Flavor Averaging Group (HFAG)** Collaboration, E. Barberio *et al.*, “Averages of b -hadron properties at the end of 2006,” [arXiv:0704.3575 \[hep-ex\]](#).
- [70] **CDF** Collaboration, T. Aaltonen *et al.*, “Search for $B_s^0 \rightarrow \mu^+ \mu^-$ and $B_d^0 \rightarrow \mu^+ \mu^-$ decays with $2fb^{-1}$ of $p\bar{p}$ collisions,” *Phys. Rev. Lett.* **100** (2008) 101802, [arXiv:0712.1708 \[hep-ex\]](#).
- [71] M. Misiak *et al.*, “The first estimate of $B(\bar{B} \rightarrow X_s \gamma)$ at $\mathcal{O}(\alpha_s^2)$,” *Phys. Rev. Lett.* **98** (2007) 022002, [arXiv:hep-ph/0609232](#).
- [72] M. Misiak and M. Steinhauser, “NNLO QCD corrections to the $B \rightarrow X_s \gamma$ matrix elements using interpolation in m_c ,” *Nucl. Phys.* **B764** (2007) 62–82, [arXiv:hep-ph/0609241](#).
- [73] F. Jegerlehner and A. Nyffeler, “The Muon g-2,” *Phys. Rept.* **477** (2009) 1–110, [arXiv:0902.3360 \[hep-ph\]](#).
- [74] M. Dine, N. Seiberg, and S. Thomas, “Higgs Physics as a Window Beyond the MSSM (BMSSM),” *Phys. Rev.* **D76** (2007) 095004, [arXiv:0707.0005 \[hep-ph\]](#).
- [75] T. Falk, K. A. Olive, L. Roszkowski, and M. Srednicki, “New Constraints on Superpartner Masses,” *Phys. Lett.* **B367** (1996) 183–187, [arXiv:hep-ph/9510308](#).
- [76] A. Kusenko, P. Langacker, and G. Segre, “Phase Transitions and Vacuum Tunneling Into Charge and Color Breaking Minima in the MSSM,” *Phys. Rev.* **D54** (1996) 5824–5834, [arXiv:hep-ph/9602414](#).
- [77] J. L. Feng, A. Rajaraman, and B. T. Smith, “Minimal supergravity with $m_0^2 < 0$,” *Phys. Rev.* **D74** (2006) 015013, [arXiv:hep-ph/0512172](#).
- [78] A. Rajaraman and B. T. Smith, “Discovering SUSY with $m_0^2 < 0$ in the first CERN LHC physics run,” *Phys. Rev.* **D75** (2007) 115015, [arXiv:hep-ph/0612235](#).
- [79] J. R. Ellis, J. Giedt, O. Lebedev, K. Olive, and M. Srednicki, “Against Tachyophobia,” *Phys. Rev.* **D78** (2008) 075006, [arXiv:0806.3648 \[hep-ph\]](#).
- [80] J. L. Evans, D. E. Morrissey, and J. D. Wells, “Vacuum Stability with Tachyonic Boundary Higgs Masses in No-Scale Supersymmetry or Gaugino Mediation,” *Phys. Rev.* **D80** (2009) 095011, [arXiv:0812.3874 \[hep-ph\]](#).
- [81] M. M. El Kheishen, A. A. Aboshousha, and A. A. Shafik, “Analytic formulas for the neutralino masses and the neutralino mixing matrix,” *Phys. Rev.* **D45** (1992) 4345–4348.
- [82] N. Arkani-Hamed, A. Delgado, and G. F. Giudice, “The well-tempered neutralino,” *Nucl. Phys.* **B741** (2006) 108–130, [arXiv:hep-ph/0601041](#).

- [83] M. A. Shifman, A. I. Vainshtein, and V. I. Zakharov, “Remarks on Higgs Boson Interactions with Nucleons,” *Phys. Lett.* **B78** (1978) 443.
- [84] J. Giedt, A. W. Thomas, and R. D. Young, “Dark matter, the CMSSM and lattice QCD,” *Phys. Rev. Lett.* **103** (2009) 201802, [arXiv:0907.4177 \[hep-ph\]](#).
- [85] J. R. Ellis, A. Ferstl, and K. A. Olive, “Exploration of elastic scattering rates for supersymmetric dark matter,” *Phys. Rev.* **D63** (2001) 065016, [arXiv:hep-ph/0007113](#).
- [86] T. Falk, A. Ferstl, and K. A. Olive, “Variations of the neutralino elastic cross-section with CP violating phases,” *Astropart. Phys.* **13** (2000) 301–316, [arXiv:hep-ph/9908311](#).
- [87] J. L. Feng, J.-F. Grivaz, and J. Nachtman, “Searches for Supersymmetry at High-Energy Colliders,” *Rev. Mod. Phys.* **82** (2010) 699–727, [arXiv:0903.0046 \[hep-ex\]](#).
- [88] S. Fiorucci *et al.*, “Status of the LUX Dark Matter Search,” *AIP Conf. Proc.* **1200** (2010) 977–980, [arXiv:0912.0482 \[astro-ph.CO\]](#).
- [89] “LUX Dark Matter Experiment website.” <http://lux.brown.edu>.
- [90] S. Dimopoulos and G. F. Giudice, “Naturalness constraints in supersymmetric theories with nonuniversal soft terms,” *Phys. Lett.* **B357** (1995) 573–578, [arXiv:hep-ph/9507282](#).
- [91] G. R. Dvali and A. Pomarol, “Anomalous U(1) as a mediator of supersymmetry breaking,” *Phys. Rev. Lett.* **77** (1996) 3728–3731, [arXiv:hep-ph/9607383](#).
- [92] A. G. Cohen, D. B. Kaplan, and A. E. Nelson, “The more minimal supersymmetric standard model,” *Phys. Lett.* **B388** (1996) 588–598, [arXiv:hep-ph/9607394](#).
- [93] J. L. Feng, C. F. Kolda, and N. Polonsky, “Solving the supersymmetric flavor problem with radiatively generated mass hierarchies,” *Nucl. Phys.* **B546** (1999) 3–18, [arXiv:hep-ph/9810500](#).
- [94] J. Bagger, J. L. Feng, and N. Polonsky, “Naturally heavy scalars in supersymmetric grand unified theories,” *Nucl. Phys.* **B563** (1999) 3–20, [arXiv:hep-ph/9905292](#).
- [95] T. Nihei and M. Sasagawa, “Relic density and elastic scattering cross sections of the neutralino in the MSSM with CP-violating phases,” *Phys. Rev.* **D70** (2004) 055011, [arXiv:hep-ph/0404100](#).
- [96] G. Belanger, F. Boudjema, S. Kraml, A. Pukhov, and A. Semenov, “Relic density of neutralino dark matter in the MSSM with CP violation,” *Phys. Rev.* **D73** (2006) 115007, [arXiv:hep-ph/0604150](#).
- [97] M. Kamionkowski and S. M. Koushiappas, “Galactic Substructure and Direct Detection of Dark Matter,” *Phys. Rev.* **D77** (2008) 103509, [arXiv:0801.3269 \[astro-ph\]](#).
- [98] **AMANDA** Collaboration, A. Achterberg *et al.*, “Limits on the muon flux from neutralino annihilations at the center of the Earth with AMANDA,” *Astropart. Phys.* **26** (2006) 129–139.
- [99] **IceCube** Collaboration, R. Abbasi *et al.*, “Limits on a muon flux from neutralino annihilations in the Sun with the IceCube 22-string detector,” *Phys. Rev. Lett.* **102** (2009) 201302, [arXiv:0902.2460 \[astro-ph.CO\]](#).
- [100] **IceCube** Collaboration, J. Braun, D. Hubert, *et al.*, “Searches for WIMP Dark Matter from the Sun with AMANDA,” [arXiv:0906.1615 \[astro-ph.HE\]](#).
- [101] E. Behnke *et al.*, “Improved Limits on Spin-Dependent WIMP-Proton Interactions from a Two Liter CF₃I Bubble Chamber,” *Phys. Rev. Lett.* **106** (2011) 021303, [arXiv:1008.3518 \[astro-ph.CO\]](#).

